Brine Diffusers and Shear Mortality

Philip J. W. Roberts, PhD, PE
Consulting Engineer
Atlanta, Georgia, USA

Final Report

Prepared for
Eastern Research Group

April 18, 2018

CONTENTS

Contents i
Executive Summary ii
List of Figures v
List of Tables vi
Notation vii
1. Introduction 1
2. Mixing Zone Regulations and Definitions 2
2.1 Introduction 2
2.2 Concept of a Mixing Zone 2
2.3 California Ocean Plan 3
2.3.1 Brine Mixing Zone 3
2.3.2 Dilution and Initial Dilution 6
2.4 Application to Brine Diffusers 6
3. Brine Diffusers 9
3.1 Introduction 9
3.2 Brine Diffuser Discharge Dynamics 9
3.2.1 Single Jets 9
3.2.2 Multiport Linear Diffusers 13
3.2.3 Multiport Rosette Diffusers 14
4. Shear Mortality 19
4.1 Introduction 19
4.2 Turbulence and Shear Mortality 19
4.3 Entrainment and Turbulence Scales in Jets 20
4.3.1 Introduction 20
4.3.2 Jet Properties 20
4.4 Estimation of Potentially Harmful Entrained Flow into Brine Diffuser Jets 24
4.4.1 Mortality Due to Jet Turbulence 24
4.4.2 Previous Entrainment Estimates 24
4.4.3 Diffuser Design Implications 26
4.4.4 Use of UM3 for Entrainment Calculations 26
4.4.5 Recommended Procedure for Entrainment Calculations 29
5. Example Application and Procedure for Evaluating Best Diffuser Design 31
5.1 Introduction 31
5.2 Diffuser Design 31
5.3 Design Procedure 32
5.4 Entrainment, Turbulence, and BMZ Calculations 34
5.5 Summary of Diffuser Analysis Procedures 36
5.5.1 Brine Mixing Zone Analysis Procedures 36
5.5.2 Shear Entrained Volume Step-by-step Procedure 37
References 38
Appendix A. Turbulence Effects on Organisms 40
Bibliography – Biological Effects 45
Appendix B. UM3 Simulations 47

EXECUTIVE SUMMARY

This document provides a method to design a brine diffuser that meets the salinity requirements of the Water Quality Control Plan for Ocean Waters of California (Ocean Plan) and minimizes discharge-related mortality of marine life. It also provides a method to predict the shear-related mortality and the extent of the Brine Mixing Zone (BMZ) for best designs and other proposed designs. An example of the diffuser design procedures and predictions of shear entrainment are presented.

The Ocean Plan contains requirements for brine discharges from seawater desalination plants, in particular receiving water limitations for salinity, the size of the BMZ, and mortality of all forms of marine life entrained into the turbulent diffuser jets. The BMZ is a region where salinity increments over natural background can be greater than 2 ppt. It should be minimized up to a maximum allowable distance of 100 m from the diffuser, at which point the salinity must be less than or equal to 2 ppt above natural background salinity. Entrainment of ocean water into the jets that may subject organisms to potentially harmful turbulence must be estimated and should be minimized.

The terminology of mixing zones, hydrodynamic mixing, and dilution, as it relates to the Ocean Plan, is discussed in Chapter 2. Dilution, as defined in the Ocean Plan, is different from that predicted by mathematical models, and average dilution is distinct from minimum dilution. The near field is a hydrodynamic mixing region whose processes are intimately linked to the discharge parameters. The far field is where mixing is due to naturally occurring processes, primarily oceanic turbulence.

Methods for predicting dilution from multiport linear diffusers and rosette diffusers are presented in Chapter 3. The literature on shear-induced mortality and jet turbulence is reviewed in Chapter 4 and a recommended procedure for estimating the volume of potentially harmful entrained water using the mathematical model UM3 is presented in Section 4.4.5.

An example calculation is given in Chapter 5. The steps to obtain the optimum diffuser design for an assumed discharge scenario are presented in Section 5.3. The port angles, orientation, spacing, and overall diffuser length are obtained. Then, in Section 5.4, the steps to predict the harmful entrained volume and the size of the BMZ for the optimum diffuser are given.

Upwardly inclined discharges, typical of those from brine diffusers, undergo a variety of hydrodynamic processes. They initially behave like jets, dominated by the source momentum, reach a terminal rise height, then

descend as plumes dominated by buoyancy. Following seabed impact, they transition to a horizontal turbulent density current that continues to entrain and mix until the turbulence collapses. This collapse marks the end of the near field. It is possible to design brine diffusers to meet the Ocean Plan's salinity requirement either at the impact point or at the end of the near field.

Applications of dense jet theories to multiport diffusers are presented in Chapter 3. To facilitate diffuser design, equations and methods for predicting impact and near field dilutions and other characteristics are presented for linear diffusers and rosette nozzle configurations.

Organisms entrained into diffuser jets may die due to exposure to turbulent shear. Particularly at risk are planktonic organisms that cannot swim away from the jets. Experimental evidence suggests that the main effect of turbulence on these organisms comes from small-scale eddies, known as the Kolmogorov scales, and that most damage occurs when their size is comparable to or smaller than the size of the organisms. These small eddies subject the organism to high strain rates and viscous shear stress that can cause injury or death whereas larger eddies mainly translate the organisms without causing significant shear. Incremental mortality in the jets over that due to natural oceanic turbulence may occur where the energy dissipation rate is greater than naturally occurring, i.e. where Kolmogorov scales are smaller than natural. Naturally-occurring Kolmogorov scales will vary somewhat with location but are assumed to be one mm.

The properties of jets are summarized and equations are given to predict the spatial variations of Kolmogorov scales. They are shortest near the nozzle and on the jet centerline and increase along the jet trajectory.

It is argued that shearing-related mortality will occur in the ascending flow region that is jet-like, i.e. dominated by the source momentum flux. Here, the energy dissipation rate is highest and Kolmogorov scales are smallest. The descending flow is plume-like, i.e. dominated by buoyancy. In this region, and in the horizontal flow, energy dissipation rates are much lower and mortality rates are likely to be small.

It is recommended that entrainment into the rising jet be predicted by the US EPA-developed mathematical model UM3 which is a module of the modeling suite Visual Plumes. Entrainment is computed up to the terminal rise height or to the location where the Kolmogorov scale equals one mm, whichever is closest to the nozzle. UM3 predicts the jet trajectory, which can be used to predict the Kolmogorov scales..

A worked example is given of the procedures for a 60 mgd discharge of brine concentrate into water 30 feet deep. The number of nozzles, spacing,

and diffuser length for a linear diffuser are computed assuming the salinity requirement is met at both the impact point and the end of the near field.

The entrained volume, size of BMZ, and Kolmogorov scales were computed by the recommended procedures. Meeting the salinity requirement at the impact point increases entrainment but results in a much smaller BMZ and lower salinity increment at the maximum BMZ limit. The Kolmogorov scales at the terminal rise height were much smaller than one mm. Transit times of particles entrained into the jets up to the top were estimated from the UM3-predicted trajectories. They are of the order of a few seconds.

The mortality rate of planktonic organisms exposed to turbulence for a few seconds is presently unknown. Estimates of mortality in the laboratory experiments due to longer exposures of minutes to hours range from 10% to 65%, although some taxa showed no mortality in field experiments. However, in an effort to be as environmentally protective as possible, we presume all forms of marine life in the volume of water exposed to lethal shear are killed.

LIST OF FIGURES

Figure 1. Extract from California Ocean Plan, chapter III.M.3, "Receiving Water Limitation for Salinity." State Water Resources Control Board (State Water Board) (2016). 5

Figure 2. BMZ area definition 6

Figure 3. a) LIF image and b) definition of major characteristics of an inclined dense jet. After Roberts et al. (1997). 7

Figure 4. Center-plane tracer concentrations for single dense jets at various nozzle angles from 15° to 85°. After Abessi and Roberts (2015). 11

Figure 5. Effect of nozzle angle on normalized impact and near field dilutions of single dense jets. After Abessi and Roberts (2015). 12

Figure 6. Effect of nozzle angle on normalized lengths of impact point, x_i/Fd, and near field, x_n/Fd, for single dense jets. After Abessi and Roberts (2015) 12

Figure 7. Effect of nozzle angle on normalized rise height y_t/Fd for single dense jets. After Abessi and Roberts (2015). 12

Figure 8. Schematic depiction of discharge from a multiport linear diffuser. After Abessi and Roberts (2014). 13

Figure 9. LIF image of discharge from a multiport linear diffuser with closely-spaced jets, s/Fd = 0.6. After Abessi and Roberts (2014). 14

Figure 10. The effect of port spacing on dilution and other properties of dense jets discharged from multiport linear diffusers. After Abessi and Roberts (2014). ..15

Figure 11. Images of four-port riser jets. From Abessi et al. (2016). 16

Figure 12. General curves for impact and near field dilutions of a single multiport rosette diffuser as functions of number of ports and nozzle angle. 17

Figure 13. LIF image and main properties of a jet 21

Figure 14. Typical UM3 graphical output for a 60° dense jet. The outer curves are the jet boundaries and the intermediate curve is the jet centerline. S_t is the dilution at the terminal rise height, the impact dilution S_i is the dilution at the nozzle height (sometimes called the return point). 27

Figure 15. UM3 predictions at the impact point and comparisons with experimental data. 29

LIST OF TABLES

Table 1. Outfall Mixing and Mixing Zone Terminology (After Roberts et al. 2010) 3
Table 2. UM3 Simulations of Single Dense Jets..... 28
Table 3. Summary of Diffuser Designs for Trial Case..... 34
Table 4. Summary of Entrainment, Kolmogorov Scales, and BMZ Areas for Trial Case .. 35

NOTATION

b_w = measure of jet width (Eqs. 26 and 27)
d = nozzle diameter or diameter of round nozzle of equivalent area to a check valve nozzle
D_m = dilution as defined in the Ocean Plan ($D_m = S - 1$)
g = acceleration due to gravity
g'_o = g'_o modified acceleration due to gravity = $g(\rho_o - \rho_a)/\rho_a$
F = jet densimetric Froude number = $u/\sqrt{g'_o d}$
H = water depth
l = size of largest (energy-containing) turbulent eddies
L = diffuser length
n = number of ports in multiport diffuser
Q = volume flow rate in jet = $Q_j + Q_e$
Q_e = volume flow rate entrained into the jet
Q_j = flow rate from an individual jet
Q_T = total flow through diffuser
r = radial distance from jet centerline (Figure 13)
R = distance from diffuser to BMZ (Figure 2)
Re = jet Reynolds number = ud/ν
s_p = port spacing (Figure 8)
S = dilution
S_a = average dilution
S_i = impact dilution (Figure 3)
S_t = centerline dilution at jet terminal rise height (Figure 3)
S_n = near field dilution (Figure 3)
S_{ta} = average dilution at jet terminal rise height predicted by UM3
u = jet exit velocity
u_e = velocity of entrained flow
u_m = jet centerline velocity
u_o = velocity of entrained flow at radial distance $r = b_w$
$\tilde{u}$ = root-mean-square (RMS) value of turbulent velocity fluctuations
w = half-width of jet
x = distance neared along jet centerline (Figure 13)
x_i = impact distance (Figure 3)
x_n = length of near field (Figure 3)
y_L = thickness of bottom-spreading layer (Figure 3)
y_t = jet terminal rise height (Figure 3)
α = entrainment coefficient
ε = energy dissipation rate

η_C	=	Kolmogorov scale on jet centerline
ρ_o	=	effluent density
ρ_a	=	ambient density
ν	=	kinematic viscosity
χ	=	distance measured along jet centerline from origin
Θ	=	angle of jet to horizontal (Figure 3)

1. INTRODUCTION

Desalination of seawater to produce potable water results in a brine that is often disposed of back into the ocean. The commonly used Reverse Osmosis (RO) process produces brine and potable water in roughly equal quantities, so the brine's salinity is about twice that of the receiving ocean water. This may be toxic to some marine organisms so the brine must be diluted to reduce its salinity to safe levels. Diffusers can accomplish this, and several desalination plants currently being contemplated or under design in California utilize them. The diffusers consist of high-speed jets that entrain ambient seawater, thereby diluting the brine and reducing its salinity. Well-designed diffusers can reduce salinity to safe levels rapidly within a short distance from the diffuser.

The Water Quality Control Plan for Ocean Waters of California (Ocean Plan) contains requirements to address brine discharges from desalination facilities. These include limitations on salinity that must be met at the edge of a designated Brine Mixing Zone (BMZ), whose extent should be minimized and shall not exceed 100 meters (328 feet) laterally from the points of discharge and throughout the water column. In addition, mortality due to turbulence of organisms entrained into the diffuser jets should be minimized and its magnitude estimated. There is presently no general method to estimate shear mortality for arbitrary diffuser designs.

The purpose of this report is to address issues in the Ocean Plan related to brine diffusers. The Ocean Plan's requirements are first discussed and how they apply to definitions of dilution and mixing zones and their prediction. Brine diffuser designs for typical multiport diffuser designs are then presented along with methods to predict dilutions and the extent of the BMZ. A suggested method is then presented to predict the volume of water that is entrained into the jets that may be subject to damaging turbulence. Finally, an example of how to apply these methods to predict dilution and entrainment for a typical diffuser is presented.

2. Mixing Zone Regulations and Definitions

2.1 Introduction

The language of mixing zones and hydrodynamic mixing of wastewater discharges has much terminology, often used interchangeably and often only vaguely defined. In this section, we attempt to clarify the terminology as it relates to wastewater discharges in general (Section 2.2) and brine discharges per the Ocean Plan.

2.2 Concept of a Mixing Zone

A mixing zone is a region where pollutants are allowed to exceed regulatory limits. Within this zone the discharge undergoes energetic mixing that can rapidly reduce the concentrations of contaminants. Mixing for a diffuser results from the turbulence generated by the high velocity of the jets issuing from nozzles and by density differences that cause effluent to either rise through the water column (in the case of a buoyant effluent such as domestic wastewater) or descend to the seabed (in the case of a dense brine discharge). This turbulence entrains ocean water that mixes with and dilutes the effluent within a few minutes after discharge and within a few tens of meters from the diffuser.

The concept of a regulatory mixing zone acknowledges this rapid and substantial contaminant reduction. For example, the US EPA regulations for toxics (USEPA 1991), defines a mixing zone as:

> *"An area where an effluent discharge undergoes initial dilution and is extended to cover the secondary mixing in the ambient water body. A mixing zone is an allocated impact zone where water quality criteria can be exceeded as long as acutely toxic conditions are prevented."*

Thus, water quality criteria are met at the mixing zone edge rather than by end-of-pipe requirements.

Table 1 summarizes some of the common terminology associated with wastewater mixing processes and the regulations that cover them. Unfortunately, there do not appear to be universal definitions of these terms, which are often used interchangeably and imprecisely. They include zone of initial dilution, regulatory and hydrodynamic mixing zones, and near and far field mixing.

Near and far field are hydrodynamic terms differentiated by the processes that effect mixing and dilution. In the near field they include shear entrainment, turbulent mixing, internal hydraulic jumps, transition to horizontal flow, and entrainment by coherent vortices in the horizontal flow. These processes are intimately linked to the discharge parameters and are under the control of the designer. Mixing in the far field is due to natural processes, primarily ambient turbulence, which are not under the influence of the designer.

Table 1. Outfall Mixing and Mixing Zone Terminology (After Roberts et al. 2010)

Term	Usage	Comments
Mixing zone	A limited area where rapid mixing takes place and where numeric water quality criteria can be exceeded but acutely toxic conditions must be prevented. Specified dilution factors and water quality requirements must be met at the edge of the mixing zone	
Allocated impact zone (AIZ)	Same as a mixing zone	
Regulatory mixing zone	As defined by the appropriate regulatory authority	Can be a length, an area, or a volume of the water body
Legal mixing zone (LMZ)	Same as a regulatory mixing zone	
Near field	Region where mixing is caused by turbulence and other processes generated by the discharge itself	Near field processes are intimately linked to the discharge parameters and are under the control of the designer. For further discussion, see Roberts et al. 2010 Chapter 3, and Doneker and Jirka (1999), and Roberts (1999c)
Hydrodynamic mixing zone	Same as near field	The near field and the hydrodynamic mixing zone are synonymous with these definitions
Far field	Region where mixing is due to ambient oceanic turbulence	Far field processes are not under control of the designer
Toxic dilution zone (TDZ)	A more restrictive mixing zone within the usual mixing zone	
Initial dilution	No specific definition	A general term for the rapid dilution that occurs near the diffuser
Zone of initial dilution (ZID)	A region extending over the water column and extending a horizontal distance of one water depth around the diffuser.	A regulatory mixing zone, as defined in the U.S. EPA's 301(h) regulations (USEPA 1994)

The regulatory mixing zone may not correspond to actual hydrodynamic mixing processes. It may fully encompass the near field and extend some distance into the far field, or it may not even fully contain the near field. Mixing zones can be defined as lengths, areas, or water volumes.

2.3 California Ocean Plan

2.3.1 Brine Mixing Zone

The Ocean Plan contains requirements in chapter III.M to address desalination facilities. The most relevant of these to the present report relate to salinity and shear mortality to aquatic organisms.

The salinity requirements are contained in chapter III.M.3, "Receiving Water Limitation for Salinity" which is reproduced in Figure 1. In addition, Appendix I of the Ocean Plan defines a BMZ as:

> *"…the area where salinity may exceed 2.0 parts per thousand above natural background salinity, or the concentration of salinity approved as part of an alternative receiving water limitation. The standard brine mixing zone shall not exceed 100 meters (328 feet) laterally from the points of discharge and throughout the water column. An alternative brine mixing zone, if approved as described in chapter III.M.3.d, shall not exceed 200 meters (656 feet) laterally from the points of discharge and throughout the water column. The brine mixing zone is an allocated impact zone where there may be toxic effects on marine life due to elevated salinity."*

The interpretation of this is that the BMZ is the area in which the salinity may exceed 2 ppt over natural background. The maximum allowable extent of the BMZ is 100 m from each point of discharge from the diffuser in any direction with no vertical limit.

The BMZ for a linear diffuser is therefore interpreted as in Figure 2, where L is the diffuser length (end port to end port) and r the distance to the 2 ppt salinity isocontour.

Other considerations related to the BMZ and shear mortality are contained in chapter III.M.2.d.(2)(b), which states that:

> *"Multiport diffusers are the next best method for disposing of brine when the brine cannot be diluted by wastewater and when there are no live organisms in the discharge. Multiport diffusers shall be engineered to maximize dilution, minimize the size of the brine mixing zone, minimize the suspension of benthic sediments, and minimize mortality of all forms of marine life."*

and in chapter III.M.2.e.(1)(b):

> *"For operational mortality related to discharges, the report shall estimate the area in which salinity exceeds 2.0 parts per thousand above natural background salinity or a facility-specific alternative receiving water limitation (see chapter III.M.3). The area in excess of the receiving water limitation for salinity shall be determined by modeling and confirmed with monitoring. The report shall use any acceptable approach approved by the regional water board for evaluating mortality that occurs due to shearing stress resulting from the facility's discharge, including any incremental increase in mortality resulting from a commingled discharge."*

3. Receiving Water Limitation for Salinity*

a. Chapter III.M.3 is applicable to all desalination facilities discharging brine* into ocean waters,* including facilities that commingle brine* and wastewater.

b. The receiving water limitation for salinity* shall be established as described below:

(1) Discharges shall not exceed a daily maximum of 2.0 parts per thousand (ppt) above natural background salinity* measured no further than 100 meters (328 ft) horizontally from each discharge point. There is no vertical limit to this zone.

(2) In determining an effluent limit necessary to meet this receiving water limitation, permit writers shall use the formula in chapter III.C.4 that has been modified for brine* discharges as follows:

Equation 1: Ce= Co + Dm(2.0 ppt)
Ce= (2.0 ppt + Cs) + Dm(2.0 ppt)

Where:

Ce= the effluent concentration limit, ppt
Co= the salinity* concentration to be met at the completion of initial* dilution= 2.0 ppt + Cs
Cs= the natural background salinity,* ppt
Dm= minimum probable initial dilution* expressed as parts seawater* per part brine* discharge

(a) The fixed distance referenced in the initial dilution* definition shall be no more than 100 meters (328 feet).

(b) In addition, the owner or operator shall develop a dilution factor (Dm) based on the distance of 100 meters (328 feet) or initial dilution,* whichever is smaller. The dilution factor (Dm) shall be developed within the brine mixing zone* using applicable water quality models that have been approved by the regional water boards in consultation with State Water Board staff.

(c) The value 2.0 ppt in Equation 1 is the maximum incremental increase above natural background salinity* (Cs) allowed at the edge of the brine mixing zone.* A regional water board may substitute an alternative numeric value for 2.0 ppt in Equation 1 based upon the results of a facility-specific alternative salinity* receiving water limitation study, as described in chapter III.M.3.c below.

Figure 1. Extract from California Ocean Plan, chapter III.M.3, "Receiving Water Limitation for Salinity." State Water Resources Control Board (State Water Board) (2016).

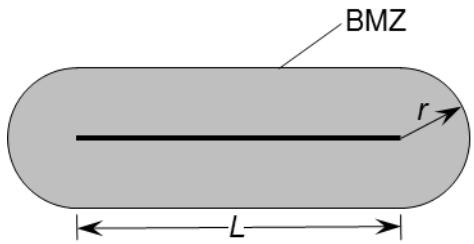

Figure 2. BMZ area definition

2.3.2 Dilution and Initial Dilution

Chapter III.M.3.b(2) (Figure 1, Equation 1) defines the dilution D_m for brine discharges as parts of seawater per part brine discharge. It should be noted that this is not the usual definition of dilution used in environmental fluid mechanics and typically outputted by numerical models such as Visual Plumes and CORMIX. This dilution, usually denoted by *S,* is defined as (Fischer et al. 1979, Eq. 1.17) the ratio of the total volume divided by the effluent volume, in other words parts of seawater plus brine per part of brine. The two definitions of dilution are related by:

$$D_m = S - 1 \tag{1}$$

The distinction should be kept in mind when interpreting the results of mathematical dilution models.

Jet and plume models also distinguish between average and minimum dilution. Average, or flux-average, dilution refers to an average over the jet or plume cross-section; minimum dilution refers to a centerline value. The centerline value is lower than the average dilution and corresponds to where the effluent is at its highest concentration. The difference between the two is substantial and it may not always be apparent which dilution a mathematical model predicts. Here, we assume that the dilutions in Eq. 1 are minimum (i.e., centerline) values. The issue is discussed further in Sections 3 and 4.

Initial dilution is referred to in the Ocean Plan chapter III.M.3.b(2)(a), Figure 1, which states:

> *"The fixed distance referenced in the initial dilution definition shall be no more than 100 meters (328 feet)."*

It is important to note that this fixed distance restricts the size of the mixing zone but this is strictly applicable to only salinity.

2.4 Application to Brine Diffusers

This section discusses how the Ocean Plan's requirements and definitions relate to brine diffusers. Brine concentrate is more dense than seawater and is often discharged from a diffuser as high velocity upwardly-inclined jets. The high

exit velocity causes shear that entrains, or engulfs, ambient seawater, which then mixes with and dilutes the jets, resulting in rapid salinity reduction.

A laboratory image and definition sketch of the major characteristics of an inclined dense jet are shown in Figure 3. Figure 3a shows a laser-induced fluorescence (LIF) image with relative salinity levels shown in false color, ranging from red (high levels) through orange, yellow, and green to blue (low levels). Figure 3b defines the main properties of a dense jet inclined at an angle Θ to the horizontal.

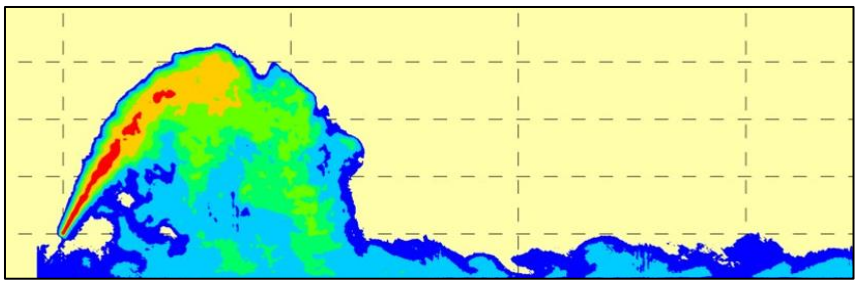

a) LIF image

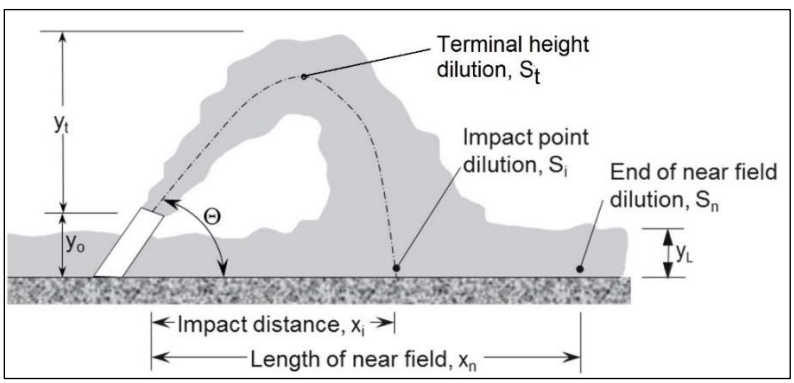

b) Major characteristics

Figure 3. a) LIF image and b) definition of major characteristics of an inclined dense jet. After Roberts et al. (1997).

The dominant hydrodynamic processes change along the flow trajectory. Initially, the discharge behaves like a jet that entrains ambient water that dilutes it. Because the jet is more dense than the receiving water, it reaches a terminal rise height y_t where the centerline dilution is S_t. It then descends as a plume with continuing entrainment and dilution. The centerline of the descending plume, where it impacts the bed, is called the impact point, and the dilution there is the impact dilution, S_i. The distance from the nozzle to the impact point is x_i. After impacting the bed, the flow becomes horizontal and proceeds as a turbulent density current that continues to entrain and dilute. Eventually, the turbulence collapses under the influence of its self-induced density stratification, and active mixing essentially ceases. This collapse signifies the end of the near field. It occurs

at a distance x_n (the length of the near field), where the dilution is the near field dilution, S_n. The increase in dilution from the impact point to the end of the near field can be substantial.

The near field for this case therefore encompasses the ascending jet and the descending plume and extends beyond the seabed impact point to include the horizontal flow up to the point of turbulence collapse. For typical brine diffusers, the near field will extend a few tens of meters from the diffuser where near field dilutions will range from about 15:1 to 40:1. For further discussion of the definition of the near field, especially as it applies to dense jets, see Roberts et al. (1997), and Doneker and Jirka (1999). Beyond the near field, mixing is primarily due to ambient (oceanic) turbulence. This is the far field, where mixing is much slower than in the near field.

3. BRINE DIFFUSERS

3.1 Introduction

This section discusses characteristics of and prediction methods for typical brine diffusers. These diffusers consist of upwardly inclined dense jets such as shown in Figure 3. Large discharges usually require multiport diffusers to reduce the required jet exit velocity and to avoid impacting the water surface in shallow water.

The ports are typically arranged either in a linear pattern or in multiport "rosette" risers. In a linear array, the ports are distributed along one or both sides of a nominally straight diffuser. This configuration is often used if the diffuser is a pipe laid on the seabed or buried in a shallow trench. Rosette risers, each typically containing four to nine ports, are often used if the diffuser is a tunnel or deeply buried pipeline to minimize the cost of the risers. If the water depth at the outfall site is shallow, the nozzles may be oriented less steeply than normal to avoid impacting the water surface.

Typical environmental design criteria for the diffuser are to maintain a submerged plume that does not impact or appear on the water surface and that results in a salinity increment of less than 2 ppt over background within the maximum allowable BMZ of 100 m from the diffuser. The extent of the BMZ should be minimized, the jet velocity should be minimized in order to minimize headloss, and shear and turbulence-induced mortality of organisms that may be entrained into the diffuser jets should also be minimized.

Below is a general discussion of the dynamics of discharges from single jets and multiport linear and rosette diffusers, design considerations, and methods for estimating their major characteristics, such as dilution and wastefield geometry.

3.2 Brine Diffuser Discharge Dynamics

3.2.1 Single Jets

Many experiments have been performed over the years to predict the main flow characteristics of a single dense jet (example shown in Figure 3b). For typical brine discharge conditions, the impact and near field dilutions, S_i and S_n (see Figure 3b), are given by:

$$\frac{S_i}{F} = f\left(\Theta\right) \quad \text{and} \quad \frac{S_n}{F} = f\left(\Theta\right) \tag{2ab}$$

where Θ is the nozzle angle and F is the densimetric jet Froude number (also referred to simply as the Froude number) defined by:

$$F = \frac{u}{\sqrt{g'_o d}} \tag{3}$$

where d is the port diameter, u the jet exit velocity, $g'_o = g\left(\rho_o - \rho_a\right)/\rho_a$, is the modified acceleration due to gravity, g the acceleration due to gravity, ρ_a the ambient density, and ρ_o the effluent density ($\rho_o > \rho_a$). The geometrical properties y_t, x_i, and x_n scale with the product of F and d:

$$\frac{y_t}{Fd} = f\left(\Theta\right) \quad \text{and} \quad \frac{x_i}{Fd} = f\left(\Theta\right) \quad \text{and} \quad \frac{x_n}{Fd} = f\left(\Theta\right) \tag{4abc}$$

Experiments on 60° jets are reported in Roberts et al. (1997) who give the values of the constants in Eqs. 2 and 4 as:

$$\frac{S_i}{F} = 1.6 \quad \text{and} \quad \frac{S_n}{F} = 2.6 \tag{5ab}$$

$$\frac{y_t}{Fd} = 2.2 \quad \text{and} \quad \frac{x_i}{Fd} = 2.4 \quad \text{and} \quad \frac{x_n}{Fd} = 9.0 \tag{6abc}$$

Eqs. 5 and 6 can be used to estimate the main characteristics of 60° jets, which is the usual design orientation.

Other nozzle angles have recently been investigated by Abessi and Roberts (2015). Figure 4 shows central-plane tracer concentrations obtained by LIF for nozzle angles Θ ranging from 15° to 85°. Figure 5 shows the variation with Θ of normalized impact dilution (S_i/F) and near field dilution (S_n/F) from Eq. 2. These empirical equations approximate the data:

$$\frac{S_n}{F} = -1.23\times10^{-5}\Theta^3 + 8.23\times10^{-4}\Theta^2 + 2.80\times10^{-2}\Theta + 5.37\times10^{-1} \tag{7}$$

$$\frac{S_i}{F} = -8.18\times10^{-6}\Theta^3 + 5.35\times10^{-4}\Theta^2 + 2.15\times10^{-2}\Theta + 3.33\times10^{-1} \tag{8}$$

where Θ is in degrees.

The trajectory length and dilution are maximum for Θ ≈ 60°, and this is the generally accepted value for diffuser design (Roberts et al. 1997). For very shallow angles, e.g. 15°, the trajectory is shortened, reducing dilution. For steep angles, e.g. 85°, the trajectory is also shortened and the jet falls back on itself, reducing dilution. The increase in dilution from the impact point to the end of the near field ranges from 30 to 60%, depending on the nozzle angle.

The geometrical properties normalized according to Eq. 4 (y_t/Fd, x_i/Fd, and x_n/Fd), are shown in Figures 6 and 7. The maximum distance of the impact point and the near field length occur at Θ ≈ 40°. The rise height increases with Θ up to about 75° beyond which it decreases slightly due to reentrainment of the ascending plume. These empirical equations approximate the data:

$$\frac{x_i}{Fd} = -1.24\times10^{-3}\Theta^2 + 9.39\times10^{-2}\Theta + 1.84 \tag{9}$$

$$\frac{x_n}{Fd} = -2.26\times10^{-3}\Theta^2 + 1.82\times10^{-1}\Theta + 7.43 \tag{10}$$

$$\frac{y_t}{Fd} = -9.98\times10^{-6}\Theta^3 + 1.24\times10^{-3}\Theta^2 - 1.01\times10^{-2}\Theta + 6.29\times10^{-1} \tag{11}$$

where Θ is in degrees.

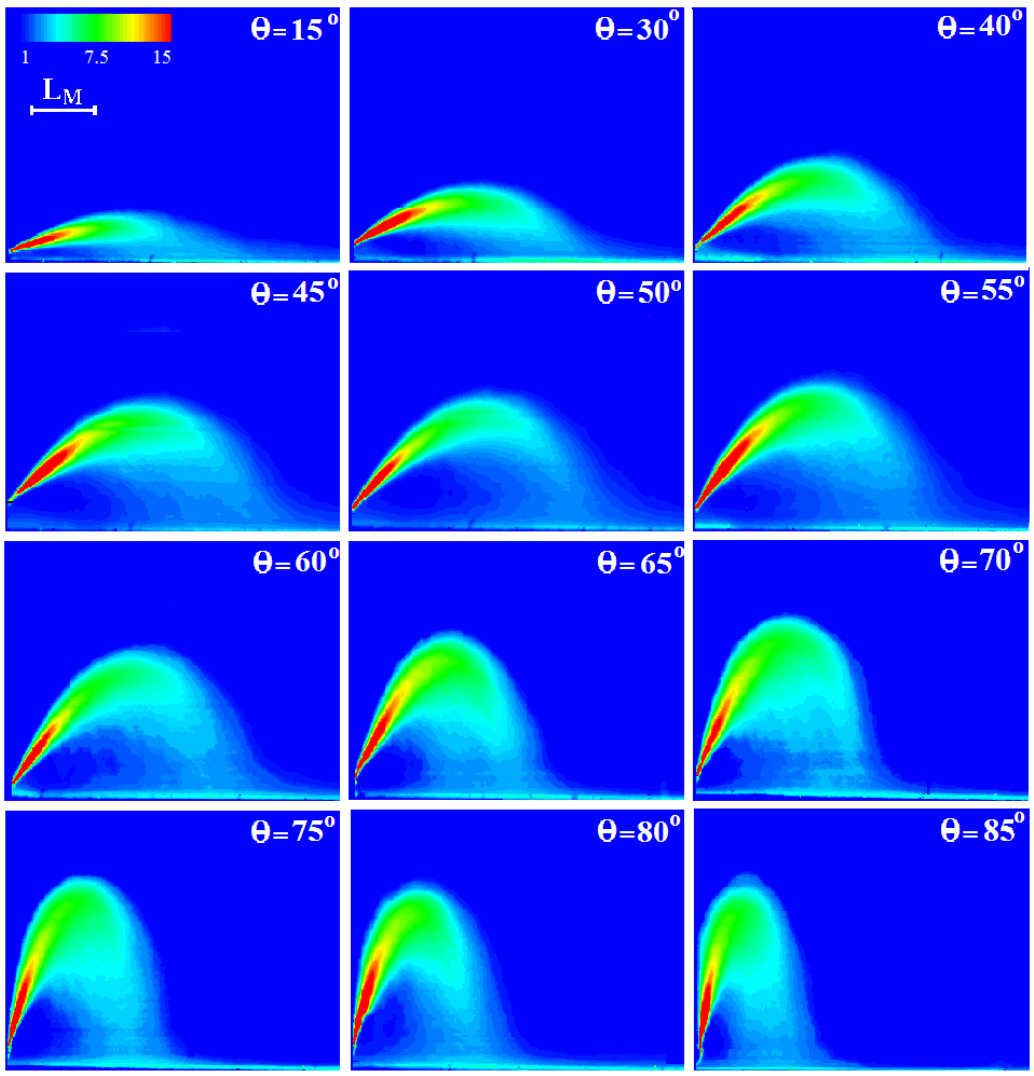

Figure 4. Center-plane tracer concentrations for single dense jets at various nozzle angles from 15° to 85°. After Abessi and Roberts (2015).

According to Abessi and Roberts (2015) the top of the jet, y_t, can be as much as 90% of the water depth with no influence of the water surface on dilution. Moving the top of the jet closer to the water surface reduces dilution.

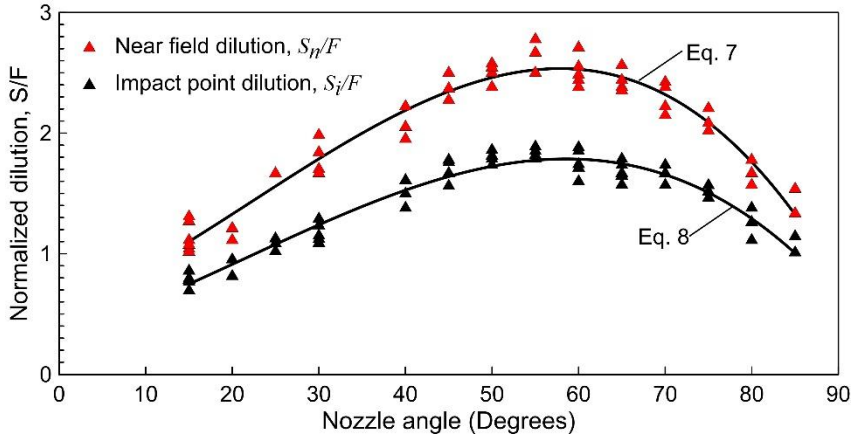

Figure 5. Effect of nozzle angle on normalized impact and near field dilutions of single dense jets. After Abessi and Roberts (2015).

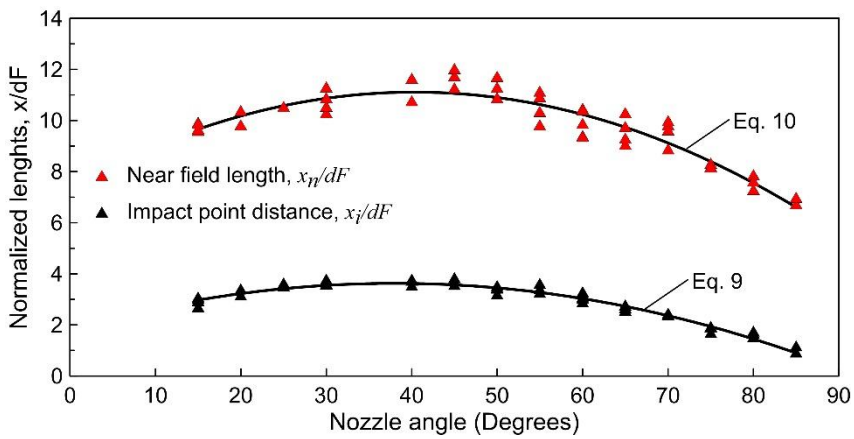

Figure 6. Effect of nozzle angle on normalized lengths of impact point, x_i/Fd, and near field, x_n/Fd, for single dense jets. After Abessi and Roberts (2015)

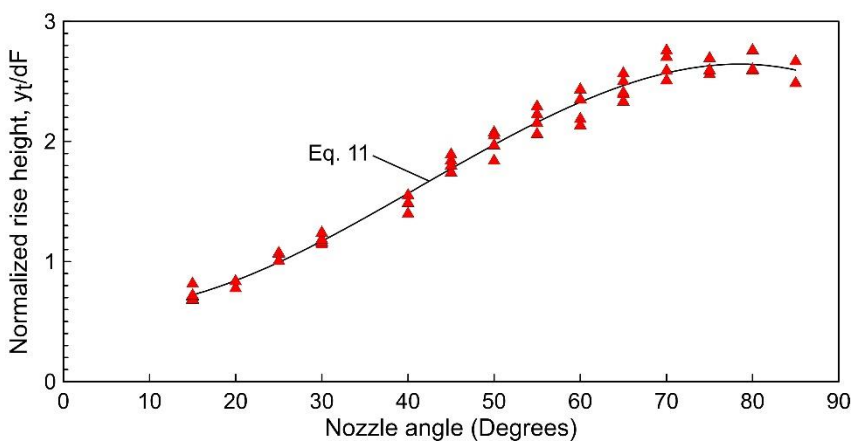

Figure 7. Effect of nozzle angle on normalized rise height y_t/Fd for single dense jets. After Abessi and Roberts (2015).

3.2.2 Multiport Linear Diffusers

Multiport linear diffusers, Figure 8, are generally used if the diffuser pipe is laid on the seabed or buried in a shallow trench. An example is Perth, Australia, Marti et al. (2011). The ports may discharge to one or both sides of the diffuser. This introduces a new parameter, s_p, the port spacing, and therefore a new dimensionless parameter, s_p/Fd. The effect of port spacing on linear diffusers discharging from one or both sides into stationary environments was investigated by Abessi and Roberts (2014).

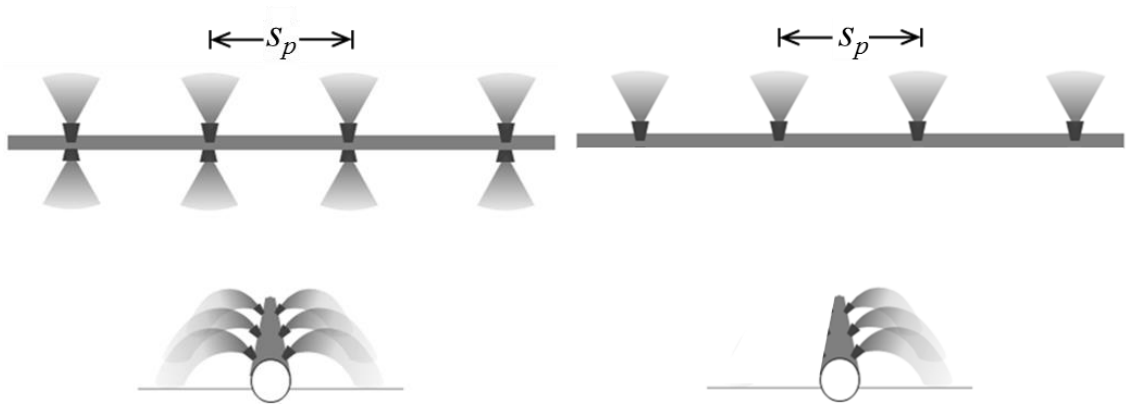

a) Discharge from both sides **b) Discharge from one side**

Figure 8. Schematic depiction of discharge from a multiport linear diffuser. After Abessi and Roberts (2014).

For a multiport linear diffuser, Eqs. 2 and 4 then become:

$$\frac{S_i}{F} = f\left(\Theta, \frac{s_p}{Fd}\right) \quad \text{and} \quad \frac{S_n}{F} = f\left(\Theta, \frac{s_p}{Fd}\right) \tag{12ab}$$

$$\frac{y_t}{Fd} = f\left(\Theta, \frac{s_p}{Fd}\right) \quad \text{and} \quad \frac{x_i}{Fd} = f\left(\Theta, \frac{s_p}{Fd}\right) \quad \text{and} \quad \frac{x_n}{Fd} = f\left(\Theta, \frac{s_p}{Fd}\right) \tag{13abc}$$

The parameter s_p/Fd describes the effect of port spacing on the jets and is discussed in Abessi and Roberts (2014). For $s_p/Fd >> 1$ the ports are widely spaced, and the jets do not merge or interfere. The solutions then approach those for the single jet, Eqs. 5 and 6. For $s_p/Fd << 1$ the jets merge and behave like a slot source reducing dilution.

This effect is illustrated by Figure 9, which is a 3D LIF image of jets with narrow spacing, $s_p/Fd = 0.6$, discharging from both sides of a diffuser. The rapid jet merging prevents entraining water from penetrating into the inner core between the ascending and descending jets. This causes a sharp reduction in dilution and rise height as the ascending and descending jets interact and entrain each other.

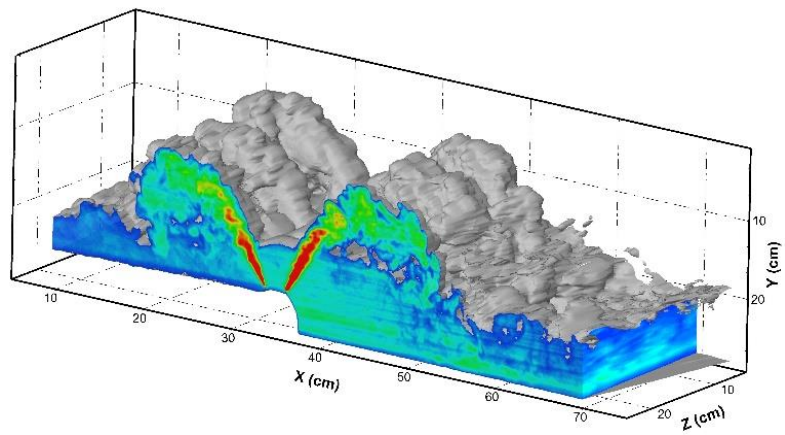

Figure 9. LIF image of discharge from a multiport linear diffuser with closely-spaced jets, *s/Fd* = 0.6. After Abessi and Roberts (2014).

The experimental results in Figure 10 show these effects. The dimensionless parameters generally become independent of port spacing for $s_p/Fd > \sim 2$, so the single jet Eqs. 5 and 6 apply. Narrower spacing results in a precipitous decline in dilution and all other dimensionless properties due to the inhibition of entrainment. Suggested equations for $s_p/Fd < \sim 2$ to enable predictions for arbitrary port spacings are shown on Figure 10.

Diffusers should, therefore, normally be designed with $s_p/Fd \geq 2$. There are no experiments for multiport diffusers with jet angles other than 60°, but it would be reasonable to use the results for single jets in Section 3.2.1 (Figures 5, 6, and 7), provided the port spacing is such that $s_p/Fd > \sim 2$.

3.2.3 Multiport Rosette Diffusers

Multiport "rosette" diffusers, where more than two nozzles are clustered on top of a riser, are often used if the outfall is tunneled in order to minimize the number of risers and therefore the construction cost. Several desalination plants in Australia employ rosette-type diffusers, e.g. Melbourne and Sydney. If the water depth at the structure is relatively shallow, the nozzles may be oriented at $\Theta < 60°$ to avoid impacting the water surface.

There are no general analytical techniques or models for predicting the dilution of a multiport rosette diffuser with an arbitrary number of ports discharging at an arbitrary angle to the horizontal. For these reasons, physical model tests (Miller et al. 2007, Tarrade and Miller 2010) are often used for specific rosette diffuser designs, and generic experiments (e.g. Abessi et al. 2016) provide some insight into rosette discharge behavior. Although it would be expected that adding more ports would increase dilution, these experiments showed that increasing the number of ports in a rosette above about six results in jet merging and inhibition of entrainment that reduces dilution. Similar effects on multiport

rosettes were reported in model studies on the Boston outfall (Roberts and Snyder, 1993), which resulted in reducing the number of ports per riser from 12 to 8.

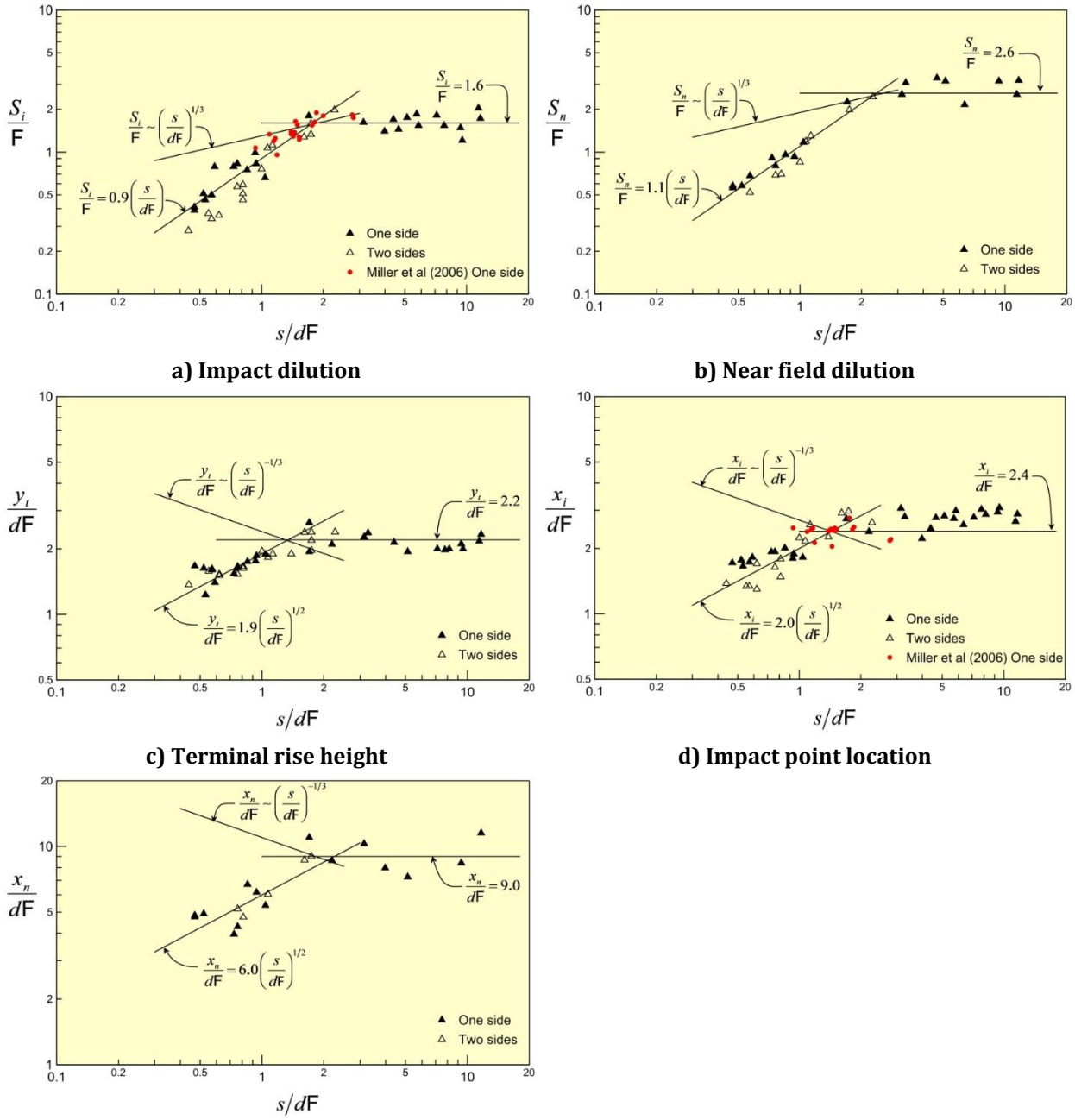

Figure 10. The effect of port spacing on dilution and other properties of dense jets discharged from multiport linear diffusers. After Abessi and Roberts (2014).

Given these effects and the limitations of mathematical models, the approach adopted here is to use experimental studies of the effect of nozzle angle on dilution for single jets with corrections that account for the reduction in dilution due to merging as the number of ports is increased. The correction factors are based on experimental studies of multiport rosettes.

For a single rosette riser, i.e. one spaced far from other risers so that they do not interact, Eq. 2 becomes:

$$\frac{S_i}{F} = f\left(\Theta, n\right) \quad \text{and} \quad \frac{S_n}{F} = f\left(\Theta, n\right) \tag{14ab}$$

where n is the number of ports on the riser.

The form of Eq. 14 can be estimated from experimental studies. Abessi et al. (2016) reported extensive generic experiments on four-port rosettes. Figure 11 shows images of a rosette discharge into stationary water. The results implied that the jets from four ports are similar to single jets, although merging in the spreading layer (visible in Figure 11) reduced the near field dilution by about 27% compared to that of single jets. Physical model tests with 9 and 12 port risers were reported by Tarrade and Miller (2010). For 12-port risers, they reported that impact and near field dilutions were both reduced by about 50% compared to single jets.

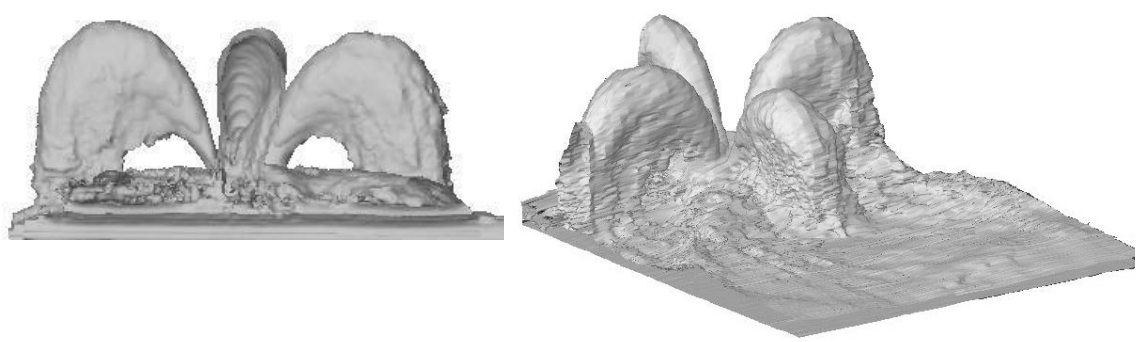

Figure 11. Images of four-port riser jets. From Abessi et al. (2016).

Based on these observations, simple linear equations were assumed for the reduction in dilution due to increasing number of ports per riser for $4 \le n \le 12$:

$$C_i = 1 - \left(\frac{n-4}{16}\right) \quad \text{and} \quad C_n = 0.73 - 0.23\left(\frac{n-4}{8}\right) \tag{15ab}$$

where the corrected impact and near field dilutions accounting for the number of ports are given by:

$$S_{ic} = C_i S_i \quad \text{and} \quad S_{nc} = C_n S_n \tag{16ab}$$

where S_i and S_n are the impact and near field dilutions for a single jet obtained from Figure 5. Substituting Eqs. 7, 8, and 15 into Eq. 16, we arrive at the generalized curves for impact and near field dilutions that account for the number of ports and their inclination that are shown in Figure 12.

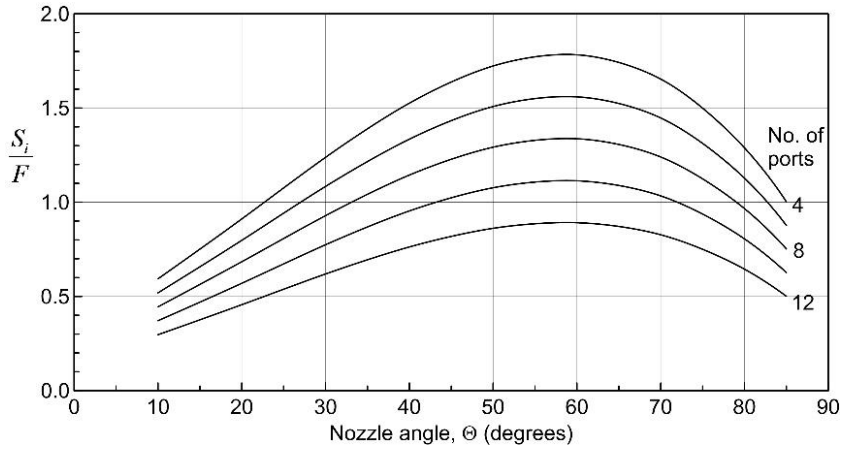

a) Impact dilution

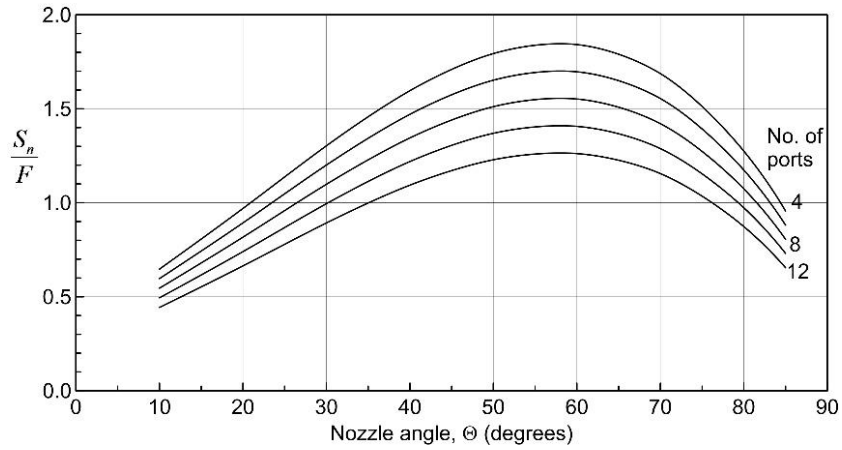

b) Near field dilution

Figure 12. General curves for impact and near field dilutions of a single multiport rosette diffuser as functions of number of ports and nozzle angle.

There are no detailed measurements of the impact point location or near field length for rosette diffusers with arbitrarily angled nozzles. Therefore, we use the results for single jets shown in Figures 6 and 7. This is a conservative assumption, as the model tests of Tarrade and Miller (2010) and the experiments of Abessi and Roberts (2014) show that these distances are generally reduced for multiport diffusers compared to single jets.

The effect of riser spacing on diffusers with multiple risers was reported in Abessi et al. (2016). They found that there was no interaction between the rosettes

if $s_r/Fd > \sim 2$, where s_r is the spacing between the riser centers. In that case, the previous results should be applicable.

4. Shear Mortality

4.1 Introduction

Chapter III.M.2.e.(1)(b) of the Ocean Plan contains the following requirement for mitigation of marine life or habitat lost due to a desalination facility:

> *"…The report shall use any acceptable approach approved by the regional water board for evaluating mortality that occurs due to shearing stress resulting from the facility's discharge, including any incremental increase in mortality resulting from a commingled discharge."*

The purpose of this section is to evaluate mortality due to the discharge. In particular, it has been suggested that planktonic organisms entrained into the high velocity turbulent jets could be subject to injury, possibly fatal, due to the effects of turbulence and shear.

4.2 Turbulence and Shear Mortality

Foster et al. (2013) reviewed the biological literature on the effects of turbulence and shear stress on aquatic organisms. The review is summarized in Appendix A.

The experimental evidence suggests that the main turbulence effect on planktonic organisms is caused by small-scale eddies, known as the Kolmogorov scales, and that most damage occurs when their size is comparable to or smaller than the size of the organisms. These small eddies subject the organism to high strain rates and viscous shear stress that can cause injury or death, whereas larger eddies mainly translate the organisms without causing significant shear. The effects vary by organism, and a number of studies on the effects of flow and turbulence on marine and freshwater organisms have been reported (Appendix A).

Most relevant here are the studies of Rehmann et al. (2003) and Jessop (2007). Rehmann et al. performed laboratory experiments in which zebra mussel veligers were subjected to controlled turbulence in beakers. They found that mortality depended on the ratio $d^* = d/\eta$, where η is the Kolmogorov size and d is the body length. Mortality increased from about 35% for $d^* < 0.9$ to about 62% for $d^* > 0.9$. That is, the mortality changed significantly when the size of the larvae was about 90% of the Kolmogorov scale. Note that, in their experiments, the mortality rate was about 35% in essentially quiescent water so the incremental mortality for $d^* > 0.9$ is less than 65%. The smallest Kolmogorov scales in these experiments corresponded to $d^* \approx 1.1$. Jessopp (2007) measured survival rates in a highly turbulent tidal channel with $0.06 < \eta < 0.25$ mm. Survival rates varied with species; thin-shelled veligers showed significant mortality of 45% to 64%, but some taxa showed no mortality.

The recent experiments of Zhang et al. (2017) further confirmed the importance of the Kolmogorov scale relative to organism size as the most important parameter in determining veliger mortality. Their study extended the range of d^* studied by Rehmann et al. from 1.1 to 3.4. Zhang's experiments were conducted in the context of enhancing mortality of golden mussel veligers by artificially generated turbulence in pipes. They performed experiments in pipelines fitted with turbulence-generating devices and measured mortality of veligers and velocity and turbulence intensity with an acoustic Doppler velocimeter. The mortality rate increased with d^*, i.e. it increases as the Kolmogorov scale becomes smaller relative to the body size. The criterion for steady killing is $d^* > 1$. Although their data showed considerable scatter, the fraction killed increased from about 10% for $d^* = 0.4$ to 25% at $d^* = 3.4$. Mortality increased in the first five minutes or so and then remained relatively constant.

4.3 Entrainment and Turbulence Scales in Jets

4.3.1 Introduction

The results of the previous section are difficult to translate to jet turbulence for a number of reasons. In the beaker experiments, the organisms were subject to homogeneous turbulence for up to 24 hours whereas in a jet organisms are subject to turbulence for a few seconds. In the field and pipeline experiments, the turbulence levels and transit times through the most turbulent regions were variable.

Turbulence in jets is not homogeneous: It varies along the jet centerline and also laterally across the jet. Kolmogorov scales are shortest near the nozzle and increase along the trajectory; they are shortest on the centerline and increase towards the jet edges. Also, transit times of entrained organisms within the jets are short, of the order of seconds, and vary according to where along the trajectory they are entrained and how they wander within the jet.

We address these issues in this section, in particular the turbulence generated by the diffuser jets and the spatial variations of turbulence intensity and length scales (eddy sizes).

4.3.2 Jet Properties

The ascending and descending portions of dense jets, Figure 3, have different dynamics. The ascending portion is driven by the source momentum flux, which is proportional to u^2d^2 where u is the jet velocity as it exits the port and d the port diameter or equivalent port diameter for a check valve. A flow driven by momentum flux only is called a jet (Fischer et al. 1979). Jets have high turbulent energy dissipation rates, therefore small Kolmogorov scales and potentially high shearing-related mortality. Density differences, or buoyancy effects, drive the descending portion. A flow driven by buoyancy flux only is called a plume. Energy

dissipation rates are much smaller in this region and are not expected to be high enough to cause mortality. The difference between the two regions can be seen in this video:

http://www.youtube.com/watch?v=TCZV2gVkpfg.

Most of the shearing-related mortality is therefore expected to occur in the ascending jet region, which is analyzed below.

Figure 13 shows an LIF image of a jet and a depiction of its main features. Close to the nozzle, the jet is fine-grained with short turbulent length scales, but these scales get larger along its trajectory. The jet entrains external fluid (and is diluted by it), and the jet width increases with distance from the nozzle.

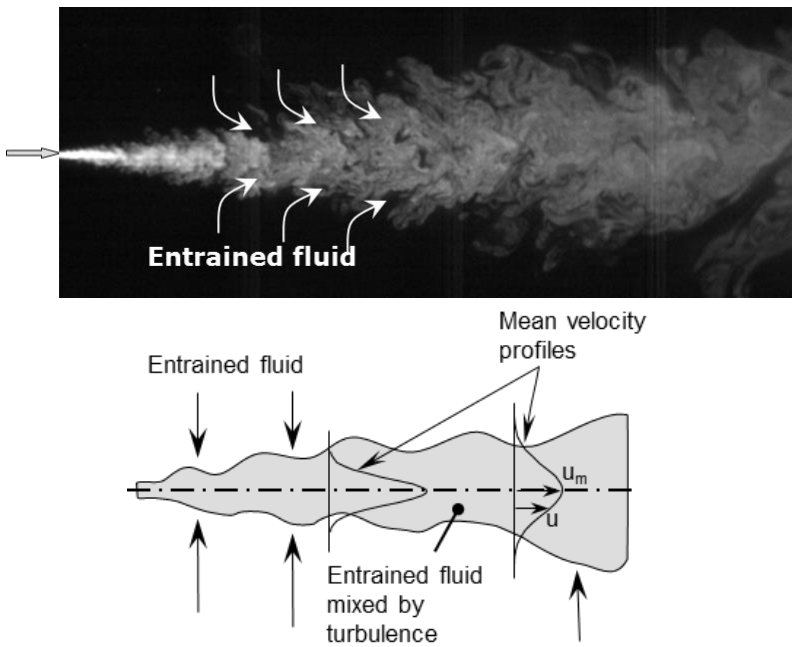

Figure 13. LIF image and main properties of a jet

The properties of round jets are well known and are summarized in Fischer et al. (1979). Close to the nozzle, there is a region known as the zone of flow establishment where the centerline jet velocity remains constant and equal to the jet exit velocity. This region extends a distance of about 6.2*d* where *d* is the port diameter. Beyond the zone of flow establishment, the profiles of velocity become closely self-similar and Gaussian and the jet properties depend only on distance *x* from the nozzle and the jet momentum flux $=(\pi/4)u^2d^2$. The centerline velocity u_m decreases rapidly with distance according to:

$$u_m = 6.2u\frac{d}{x} \tag{17}$$

The half-width of the jet w, defined as two standard deviations of a Gaussian velocity distribution, increases linearly with distance according to:

$$w = 0.15x \tag{18}$$

Combining Eqs. 17 and 18, we see that a measure of the velocity shear in the jet du/dr where u is the local velocity and r the radial distance from the jet centerline is:

$$\frac{du}{dr} \approx \frac{u_m}{w} \approx 41\frac{ud}{x^2} \tag{19}$$

So mean shear decreases even more rapidly than velocity with distance from the nozzle.

Turbulence properties can be estimated from the experimental data of Webster et al. (2001). They show the relative turbulence intensity on the centerline, $\tilde{u}/u_m \approx 0.3$ where $\tilde{u}$ is the root-mean-square (rms) value of the turbulent velocity fluctuations. The intensity decreases with radial distance to zero at the edge of the ascending jet, defined approximately by Eq. 18.

The size of the small-scale (Kolmogorov) eddies η can be estimated from:

$$\eta \sim \left(\frac{\nu^3}{\varepsilon}\right)^{1/4} \tag{20}$$

where ν is the kinematic viscosity of seawater assumed equal to 1.17×10^{-6} m²/s or 1.26×10^{-5} ft²/s and ε the energy dissipation rate which can be approximated as:

$$\varepsilon \sim \frac{\tilde{u}^3}{l_L} \tag{21}$$

where l_L is a measure of the largest (energy containing) eddies in the jet. According to Wygnanski and Fiedler (1969) these length scales also increase linearly with distance from the nozzle and vary radially across the jet. On the centerline, $l_L \sim 0.016x$, i.e. about 1/12 of the jet width.

Combining the above equations we find:

$$\frac{\eta_c}{x} = 0.24\,\mathrm{Re}^{-3/4} \tag{22}$$

where $\mathrm{Re} = ud/\nu$ is the jet Reynolds number and η_c the size of the Kolmogorov eddies on the jet centerline. The Kolmogorov scales therefore increase linearly with distance along the jet trajectory.

The radial variation of turbulence intensity and turbulent length scales across the jet is now considered. Near the jet edge, $l_L \sim 0.03x$ according to Wygnanski and Fiedler, i.e. about 1/25 of the jet width, and the turbulence intensity is about $\tilde{u}/u_m \approx 0.04$ according to Webster et al. (2001). Combining this information with

Eqs. 20 and 21, we can estimate the ratio of the Kolmogorov scale on the centerline to that at the jet edge as:

$$\frac{\eta_c}{\eta_e} = \left\{ \frac{\left(\ell_c/\ell_e\right)}{\left(\tilde{u}_c/\tilde{u}_e\right)^3} \right\}^{1/4} \approx 0.2 \tag{23}$$

where the subscripts *c* and *e* refer to the jet centerline and edge, respectively. Eq. 23 indicates that the Kolmogorov scales at the jet edge are about five times larger than on the centerline.

Travel times of entrained larvae along the jet trajectory will vary, depending on where along the trajectory they enter the jet and whether they mainly travel on the centerline, on the edge, or in between. On the centerline, the velocity varies according to Eq. 17, so the time for a particle to traverse a distance χ from the nozzle is given approximately by:

$$t = \int_0^{\chi} \frac{dx}{u_m} = \int_0^{\chi} \frac{x}{6.2ud} dx = \frac{\chi^2}{12.4ud} \tag{24}$$

The word entrainment arises in two contexts in desalination projects. It refers to flow drawn into intakes, and, in the jets and plumes that arise in brine diffusers, to the flow induced by velocity shear at the edge of the jet (see Figure 13). This flow, commonly referred to as entrained flow, mixes with and dilutes the effluent stream. In the context of this report, entrainment refers only to that which is discharge-induced.

The velocity at which flow is entrained into the jet is directly proportional to the local centerline velocity and is given by:

$$u_o = \alpha u_m \tag{25}$$

where $\alpha \approx 0.0535$ (Fischer et al. 1979) is the entrainment coefficient, u_o is the entrainment velocity at a radial distance $r = b_w$ from the jet centerline, where b_w is a measure of the jet width given by (Fischer et al. 1997):

$$b_w = 0.107x \tag{26}$$

The local velocity in the jet u at a radial distance r from the jet centerline is given by:

$$\frac{u}{u_m} = \exp\left\{ -\frac{r^2}{b_w^2} \right\} \tag{27}$$

The velocity of the external flow u_e that is entrained into the jet decreases with radial distance r and can be determined by continuity:

$$u_o 2\pi b_w = u_e 2\pi r$$

or

$$u_e = u_o \frac{b_w}{r} \tag{28}$$

Combining Eqs. 17, 25, 27, and 28, we find:

$$u_e = 6.2 \times 0.107 \alpha \frac{ud}{r}$$

and assuming $\alpha = 0.0535$ (Fischer et al. 1979), this becomes:

$$u_e = 0.035 \frac{ud}{r} \tag{29}$$

In other words, the entrainment velocity is constant with the distance along the jet, x, but decreases rapidly with radial distance from the jet centerline, r.

The volume flow rate in a jet Q is directly related to dilution and is given by (Fischer et al. 1979):

$$Q = S_a Q_j = 1.4 S_m Q_j \tag{30}$$

where Q_j is the jet discharge rate, S_a the average dilution, and S_m the minimum (centerline) dilution. The average and minimum dilutions are related by $S_a = 1.4 S_m$.

4.4 Estimation of Potentially Harmful Entrained Flow into Brine Diffuser Jets

4.4.1 Mortality Due to Jet Turbulence

Only planktonic organisms that cannot swim away from the jets are likely to be entrained so they are the main emphasis here. The biological evidence in Section 4.2 suggests that the main effect of turbulence on these organisms is mortality due to shear stresses resulting from eddies whose smallest scales (the Kolmogorov eddies) are less than or comparable to their body size. Some natural mortality due to turbulent shear will occur in the ocean so we are only interested in the incremental mortality due to the jets. This incremental mortality will occur where energy dissipation rates are greater than naturally occurring, i.e. where the Kolmogorov scales are smaller than ambient oceanic values.

There are few measurements of Kolmogorov scales in the ocean. Walter et al. (2014) reported values in Monterey Bay, California, to be about one mm. Eq. 20 shows the Kolmogorov scale to be proportional to $\varepsilon^{-1/4}$ so it is insensitive to changes in the energy dissipation rate and should not vary greatly in California coastal waters. Therefore, the region in the jets where entrained organisms may be exposed to harmful turbulence is presumed to be where the Kolmogorov scale is less than one mm.

4.4.2 Previous Entrainment Estimates

The State Water Board, in the Final Staff Report Including the Substitute Environmental Documentation for the Desalination Amendment to the Ocean

Plan (SED) (State Water Board, 2015b) that addresses desalination facilities, discussed entrainment into brine diffuser jets. The report includes an analysis from Foster et al. (2013) of the entrained water that might be subject to lethal turbulence. The analysis is summarized below.

For the particular case of a single jet at 60°, the dilutions at the terminal rise height S_t, impact point S_i, and end of near field S_n are given by (Abessi and Roberts, 2013) and Eq. 5:

$$\frac{S_t}{F} = 0.6 \quad \text{and} \quad \frac{S_i}{F} = 1.6 \quad \text{and} \quad \frac{S_n}{F} = 2.6 \tag{31abc}$$

where F is the jet densimetric Froude number (Eq. 3). For arbitrary nozzle angles, the impact and near field dilution coefficients can be calculated from Eqs. 7 and 8.

By assuming the ratio of average to minimum dilution remains constant along the flow trajectory, we can estimate from Eq. 31 the ratios of the volume of water entrained by the jet at its top (terminal rise height) to the volume entrained at the impact point and near field. The ratio at the top (terminal rise height) to that at the impact point is 0.6/1.6 = 0.38 = 38%, and the ratio at the top (terminal rise height) to that at the end of the near field is 0.6/2.6 = 0.23 = 23%. For 60° nozzles, the volume flow rate in the jet at its terminal rise height is then given by Eq. 30:

$$Q = 1.4 S_t Q_j = 1.4\left(\frac{S_t}{S_i}\right) S_i Q_j = 1.4\left(\frac{0.6}{1.6}\right) S_i Q_j = 0.53 S_i Q_j \tag{32}$$

or

$$Q = 1.4 S_t Q_j = 1.4 \times \left(\frac{S_t}{S}\right) S_n Q_j = 1.4 \times \left(\frac{0.6}{2.6}\right) S_n Q_j = 0.32 S_n Q_j \tag{33}$$

The volume flow rate in the jet is the sum of the source volume flux Q_j and the entrained volume flow Q_e: $Q = Q_j + Q_e$. So, for a total of n jets, the entrained flows into the jet up to its terminal rise height from Eqs. 32 and 33 become:

$$Q_e = n\left(0.53 S_i Q_j - Q_j\right) = n Q_j \left(0.53 S_i - 1\right) \tag{34}$$

or

$$Q_e = n\left(0.32 S_n Q_j - Q_j\right) = n Q_j \left(0.32 S_n - 1\right) \tag{35}$$

Q_e is the volume of entrained flow that is assumed to be potentially harmful to organisms carried with it. Note that Eqs. 32 through 35 apply only to 60° nozzles. Different coefficients would apply to other angles, and a more general procedure for arbitrary angles is presented in Section 4.4.4.

4.4.3 Diffuser Design Implications

It is possible to design brine diffusers to meet the Ocean Plan's salinity requirement either at the impact point or at the end of the near field. If it is met at the impact point, the required dilution is S_i and Eq. 34 applies; if it is met at the near field, the required dilution is S_n and Eq. 35 applies.

If the receiving water limit for salinity is met at the impact point, the potentially harmful entrained flow is greater because more of the required dilution occurs in the rising jet region. If it is met at the end of the near field, the volume of entrained flow exposed to lethal turbulence is less because some of the required dilution occurs in the horizontal density current that is not subject to high shear rates. Meeting the salinity requirement at the impact point results in a much smaller BMZ than if met at the near field, but meeting at the impact point requires a higher jet velocity and therefore higher head loss in the outfall. These issues are illustrated in the example calculation in Section 5.

The diffuser design with the lowest volume of entrained flow has the least mortality due to shear. However, the optimized diffuser design that meets the intent of the Ocean Plan would pose the least discharge mortality considering the combined shear mortality, expressed as area of production forgone (APF), and areal extent of the BMZ. The final procedural step to calculate the least discharge mortality to support the choice of the best diffuser design that minimizes mortality of all forms of marine life is outside the scope of this report and will require further regulatory guidance.

4.4.4 Use of UM3 for Entrainment Calculations

Equations 31 to 35 apply to a 60° jet only. We cannot apply the method to other angles as we do not in general have estimates of the terminal height dilution S_t for arbitrary angles. In addition, the ratio of average to minimum dilutions throughout the flow field is unknown.

Therefore, we recommend the use of the EPA mathematical model UM3 to predict entrained flow for other angles. UM3 was originally developed by the US EPA and has been widely used around the world. It is part of the modeling suite Visual Plumes and is freely available for download from the State Water Board at:

https://www.waterboards.ca.gov/water_issues/programs/ocean/

or https://ftp.waterboards.ca.gov/

A user's manual is available on the FTP site, and it is described in other publications such as Baumgartner et al. (1994), Frick (2004), Frick et al. (2010), and Frick and Roberts (2016).

UM3 is an entrainment model for jet and plume calculations typical of wastewater discharges from diffusers. It computes the three-dimensional trajectories of individual jets and plumes in stationary and flowing currents and stratified and unstratified environments. It has the advantage that its emphasis is

on average properties and it predicts the entrained volume flux directly. It is simple to use and is robust. For reasons discussed below, however, we do not recommend it to be used for impact or near field dilutions, but it can be used to estimate jet properties up to the terminal rise height, which is the region where shear mortality is expected to occur. These considerations and an application are discussed below.

UM3 (Version 17b) was run for a variety of typical conditions and the predictions were expressed in dimensionless form to compare with the previous experimental results (Section 3.2.1). A typical jet trajectory and plume width are shown in Figure 14 for a 60° jet with Froude number $F = 24$. The height to the top of the jet at its terminal rise height y_t (Figure 3b) was computed as the centerline height at the terminal rise plus half the plume diameter. Table 2 summarizes the UM3 results in dimensional and dimensionless forms.

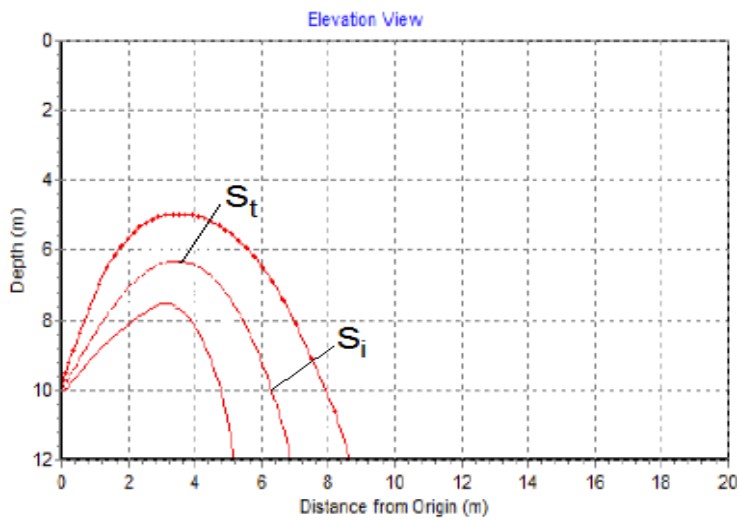

Figure 14. Typical UM3 graphical output for a 60° dense jet. The outer curves are the jet boundaries and the intermediate curve is the jet centerline. S_t is the dilution at the terminal rise height, the impact dilution S_i is the dilution at the nozzle height (sometimes called the return point).

For 60° jets, the UM3 predicted dimensionless dilutions at the terminal rise height that agree well with the experimental value $S_t/F = 0.6$ (Eq. 31). For nozzle angles ranging from 15 to 85° UM3 underestimates the normalized rise height y_t/Fd and impact distance x_i/Fd by 16 to 27%. The normalized impact dilution S_i/F for all nozzle angles is plotted in Figure 15 and compared with the previous experimental results that were shown in Figure 5. UM3 significantly underestimates the impact dilution.

Table 2. UM3 Simulations of Single Dense Jets

Jet variables						UM3 predictions							
						At top		At return point		In dimensionless form			
Diam. d (m)	Angle Θ (deg)	Flow Q_j (mgd)	Density ρ_0 (kg/m^3)	Velocity u (m/s)	Froude Number F	Dilutn S_{ta}	y_t (m)	Dilutn S_i	X_i (m)	S_t/F	y_t/Fd	S_i/F	x_i/Fd
0.15	60	1.14	1049	2.8	15.2	9.6	3.6	18.5	4.6	0.63	1.59	1.22	2.01
0.15	60	0.68	1049	1.7	9.1	5.8	2.1	10.6	2.6	0.63	1.51	1.16	1.92
0.10	60	1.14	1049	6.4	42.0	26.4	7.0	52.5	8.8	0.63	1.67	1.25	2.09
0.10	60	0.68	1049	3.8	25.2	15.8	4.1	30.7	5.2	0.63	1.64	1.22	2.05
0.15	45	1.14	1049	2.8	15.2	9.9	2.7	18.2	5.3	0.65	1.18	1.20	2.31
0.15	45	0.68	1049	1.7	9.1	6.1	1.6	10.9	3.1	0.67	1.15	1.19	2.25
0.10	45	1.14	1049	6.4	42.0	27.9	5.4	52.4	10.3	0.66	1.27	1.25	2.45
0.10	45	0.68	1049	3.8	25.2	16.7	3.1	31.5	6.1	0.66	1.25	1.25	2.43
0.15	30	1.14	1049	2.8	15.2	9.3	1.8	16.2	5.2	0.61	0.79	1.06	2.28
0.15	30	0.68	1049	1.7	9.1	5.6	1.0	9.6	3.0	0.62	0.75	1.04	2.15
0.10	30	1.14	1049	6.4	42.0	25.5	3.5	46.0	10.1	0.61	0.83	1.09	2.41
0.10	30	0.68	1049	3.8	25.2	15.3	2.1	27.3	6.0	0.61	0.81	1.08	2.36
0.15	60	1.14	1065	2.8	11.8	7.6	2.8	14.3	3.5	0.64	1.58	1.21	2.00
0.15	60	0.68	1065	1.7	7.1	4.6	1.6	8.3	2.0	0.65	1.49	1.17	1.90
0.10	60	1.14	1065	6.4	32.5	20.9	5.5	40.7	6.8	0.64	1.68	1.25	2.10
0.10	60	0.68	1065	3.8	19.5	12.5	3.2	24.4	4.0	0.64	1.64	1.25	2.07
0.15	15	1.14	1049	2.8	15.2	7.1	0.9	11.8	3.9	0.46	0.39	0.77	1.72
0.15	20	1.14	1049	2.8	15.2	8.0	1.2	13.5	4.5	0.53	0.52	0.89	1.96
0.15	70	1.14	1049	2.8	15.2	9.0	4.4	17.6	3.4	0.59	1.95	1.16	1.50
0.15	80	1.14	1049	2.8	15.2	8.8	4.9	17.3	1.8	0.57	2.12	1.14	0.81

The significant underestimation of impact dilution of dense jets by UM3 (and other entrainment models) has been previously reported by Palomar et al. (2012). Some reasons for this are that the entrainment models assume the flow to be everywhere radially symmetric whereas experimental observations show the flow to become increasingly asymmetric as the terminal rise height is approached. This asymmetry is caused by "gravitational instabilities" (heavier fluid over lighter fluid) that cause considerable internal mixing that is not accounted for in the models. In addition, the length of the jet trajectory is underestimated, providing less opportunity for entrainment along its length.

Where the flow is more jet-like and round, however, i.e. where it is dominated by source momentum during its upward trajectory, UM3 gives good dilution predictions. This was also observed in comparisons of UM3 predictions with experimentally based empirical equations for the desalination outfall in Monterey, CA (Roberts 2016), which has horizontal jets and whose dilution is momentum-dominated.

Note that, in UM3, the default predicted dilution that is labeled *Dilutn* is actually an average, or flux-average, value. The centerline dilution, denoted by *CL-diln*, is not outputted by default and must be added. For a round jet, UM3 assumes the centerline dilution is one-half of the average dilution.

Note also that UM3 does not predict near field dilution; it only applies in the free jet or plume region and not after the transition to horizontal flow or the subsequent turbulent collapse. This does not affect its ability to evaluate or predict shear mortality in the ascending jet region.

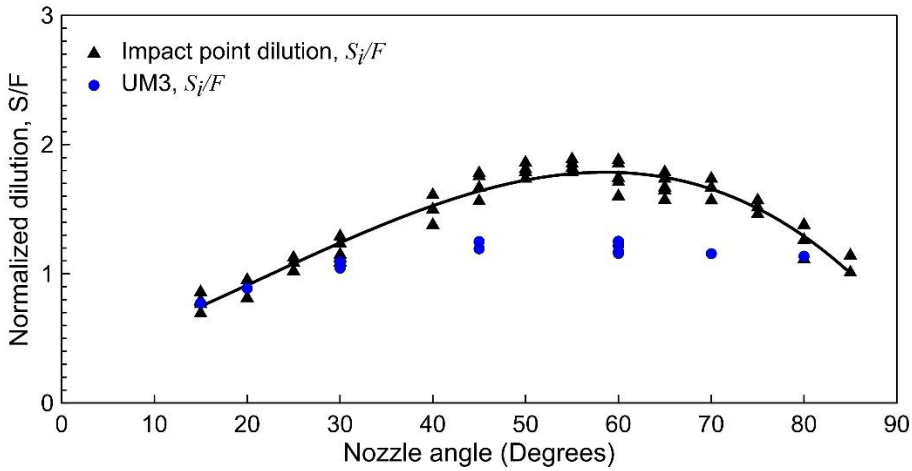

Figure 15. UM3 predictions at the impact point and comparisons with experimental data.

4.4.5 Recommended Procedure for Entrainment Calculations

It is recommended to apply UM3 to predict entrainment. Conditions at the terminal rise height are obtained at the level designated in UM3 as "local maximum rise or fall." Denoting the UM3 average dilution at this point by S_{ta}, the potentially harmful entrained volume flux Q_e is then computed from:

$$Q_e = nQ_j(S_{ta} - 1) \tag{36}$$

where n is the total number of ports and Q_j is the volume flux per port. This calculation assumes no interference or merging of the jets in the ascending region; for multiport diffusers, this is assured if $s_p/Fd > 2$ (Section 3.2.2).

The Kolmogorov scales up to the terminal rise height should be estimated from Eq. 22 where x is replaced by χ, the distance along the curved jet centerline from the nozzle to the terminal rise height. This can be obtained from the UM3 output, which provides horizontal and vertical coordinates of the jet trajectory. If the Kolmogorov length at the terminal rise height is greater than one mm, the entrained volume flux should be computed up to the point where it is equal to one mm. This point can be calculated from Eq. 22. For typical desalination diffusers,

however, the Kolmogorov scale will be less than one mm at the terminal rise height so this calculation will not be necessary.

An example calculation is given in Section 5.

5. Example Application and Procedure for Evaluating Best Diffuser Design

5.1 Introduction

This section presents an example calculation for a diffuser design and application of the recommended method for estimating the volume of entrained water that may be subject to harmful turbulent shear.

The following method can be used to determine the Best Available Diffuser Design as stated in the Ocean Plan. First, determine the best diffuser design for the project by following the steps in Section 5.3. Then evaluate discharge-related mortality for the diffuser by following the steps in Section 5.4. Then evaluate discharge-related mortality for the diffuser proposed by the project applicant by using the methods in Section 5.4. Compare estimates of mortality for the designs.

5.2 Diffuser Design

The design of a brine diffuser involves many variables: The outfall length (and therefore discharge depth), number of ports and their orientation and diameter, port spacing (and therefore diffuser length), and diffuser configuration whether the ports are in one or more multiport rosettes or arranged linearly on one or both sides of the diffuser. A full discussion of design involving all of these variables is beyond the scope of the present report and the final project will include other considerations such as local conditions, constructability and cost. Some general observations can be made however.

If possible, the nozzles should be oriented at 60° to minimize shear entrainment and jet velocity. This is the case for the following example, where the discharge depth is assumed to be prescribed and the optimum number of ports and the diffuser length are determined. If the discharge depth and diffuser length are both variables, however, there is no optimum hydraulic design - discharge into shallower water will require a longer diffuser - and other factors will come into play. If the receiving water depth is predetermined and shallow and the diffuser length constrained, such as with a single rosette riser, it may be necessary to orient the nozzles at less than 60° to prevent plume surfacing. An example of the procedure for this case is given in the companion report, Roberts (2018), Section 3.2.

For a linear diffuser the ports can discharge to one or both sides (Figure 8). Discharge to one side results in a net horizontal momentum flux that can aid in moving the mixed wastefield offshore. The diffuser length and size of the BMZ are larger. Discharge to both sides results in no net horizontal momentum flux; the diffuser is shorter and the size of the BMZ is smaller. In the following example, we assume discharge is to one side. An example of a linear diffuser with discharge to both sides is given in the companion report, Roberts (2018), Section 3.3.

5.3 Design Procedure

For this example, we assume a seawater desalination plant that produces 60 mgd (92.8 ft^3/s) of brine. The ambient ocean salinity is 34 ppt and the discharge salinity is doubled to 68 ppt. Assuming temperatures of 20°C, the ambient density ρ_a = 1024.0 kg/m^3 and the effluent density ρ_o = 1050.2 kg/m^3. The depth of the ports is assumed to be 30 ft. We assume a linear diffuser array with the ports arranged on one side as in Figure 8b.

The primary environmental design requirements are initial dilution and plume submergence. For the example scenario, a salinity increment of 2 ppt requires a dilution:

$$S = \frac{68-34}{2} = 17 \tag{37}$$

The diffuser can be designed to achieve this dilution either at the impact point or at the end of the near field; both calculations are presented here. Abessi and Roberts (2015) suggest that the rise height y_t can be up to 90% of the water depth with no effect of the free surface on dilution. Therefore, we take the maximum rise height y_t as 90% of the port depth of 30 ft, i.e. 27 ft. The following calculation is to compute the minimum number of ports required (and therefore minimum diffuser length) to achieve $y_t \leq 27$ feet and salinity after initial dilution less than 2 ppt. Increasing the number of ports above this minimum number results in lower jet velocity and rise height but does not significantly affect the entrained volume. It increases the diffuser length and possibly the size of the BMZ but the increases in BMZ size are generally on the order of 0.1 acres.

In this example, we assume the dilution S = 17 (Eq. 37) needed to meet the salinity requirement occurs at the impact point. The procedure for computing the diffuser configuration involves the following steps:

1. Calculate the required Froude number from Eq. 5a.

$$F = \frac{S}{1.6} = \frac{17}{1.6} = 10.6$$

2. Calculate the nozzle diameter from Eq. 6a:

$$d = \frac{y_t}{2.2F} = \frac{27}{2.2 \times 10.6} = 1.16 \text{ ft}$$

3. Calculate the jet exit velocity from Eq. 3:

$$u = F\sqrt{g\frac{\rho_o - \rho_a}{\rho_a}d} = 10.6\sqrt{32.2 \times \left(\frac{1050.2-1024.0}{1024.0}\right) \times 1.16} = 10.4 \text{ ft/s}$$

4. Calculate the flow from this port (velocity times port area):

$$Q_j = u\frac{\pi}{4}d^2 = 10.4\times\frac{\pi}{4}\times 1.16^2 = 11.0 \text{ ft}^3/\text{s} = 7.11 \text{ mgd}$$

5. Calculate the required number of ports n from:

$$n = \frac{Q_T}{Q_j} = \frac{92.8}{11.0} = 8.44$$

6. Because a diffuser must have an integral number of ports, we round up to the nearest whole number, so n = 9.

7. Compute the new flow per port from:

$$Q_j = \frac{Q_T}{n} = \frac{92.8}{9} = 10.3 \text{ ft}^3/\text{s} = 6.66 \text{ mgd}$$

then:

a. Recompute the port diameter d to achieve the impact dilution S_i = 17 (F = 10.6). This is done by rearranging Eq. 5 given the jet flow rate Q_j, the definition of F (Eq. 3), and jet velocity $u = 4Q_j/\pi d^2$:

$$d = \left(\frac{4Q_j}{F\pi}\right)^{2/5}\left(g\frac{\rho_o-\rho_a}{\rho_o}\right)^{-1/5}$$
$$= \left(\frac{4\times 10.3}{10.6\times\pi}\right)^{2/5}\left(32.2\times\frac{1050.2-1024.0}{1024.0}\right)^{-1/5}$$
$$= 1.13 \text{ ft}$$

b. Compute the near field dilution from Eq. 5b.

$$S_n = 2.6\times 10.6 = 28$$

c. Compute the rise height, impact distance, and the near field length from Eq. 6abc.

$$y_t = 2.2Fd = 2.2\times 10.6\times 1.13 = 26.3 \text{ ft}$$
$$x_i = 2.4Fd = 2.4\times 10.6\times 1.13 = 28.8 \text{ ft}$$
$$x_n = 9.0Fd = 9.0\times 10.6\times 1.13 = 107.8 \text{ ft}$$

8. Compute the minimum port spacing s_p to avoid jet interference (Section 3.2.2) from:

$$s_p = 2Fd = 2\times 10.6\times 1.13 = 24 \text{ ft}$$

9. Compute the diffuser length (assuming the ports are on one side of the diffuser, Figure 8b) from:

$$L = (n-1)s_p = (9-1)\times 24 = 192 \text{ ft}$$

The calculations were then repeated assuming that the dilution was met at the end of the near field using Eq. 5. Table 3 summarizes the results (for a 60° nozzle angle).

Table 3. Summary of Diffuser Designs for Trial Case

Parameter	Salinity requirement met at:	
	Impact point	End of near field
Number of ports, *n*	9	5
Port diameter, *d*	1.13 ft	1.74 ft
Jet velocity, *u*	10.3 ft/s	7.8 ft/s
Froude number, *F*	10.6	6.6
Rise height, y_t	26.3 ft	25.0 ft
Impact dilution, S_i	17	10
Near field dilution, S_n	28	17
Impact distance, x_i	28.8 ft	27.3 ft
Near field length, x_n	108 ft	102 ft
Port spacing, *s*	24 ft	24 ft
Diffuser length, *L*	192 ft	96 ft

5.4 Entrainment, Turbulence, and BMZ Calculations

UM3 was then run for the two diffuser designs in Table 3; the outputs from the two runs are given in Appendix B. The dilutions S_{ta} at the terminal rise height are 6.71 and 4.22 respectively. The steps to compute entrainment are:

1. Compute the jet Reynolds number from:

$$\text{Re} = \frac{ud}{\nu} = \frac{10.3\times 1.13}{1.26\times 10^{-5}} = 9.2\times 10^5$$

2. Compute the jet path length from nozzle to the terminal rise height from the tabulated trajectory output in Appendix B from:

$$\chi = \sum_{i=1}^{j} \sqrt{(\Delta x)^2 + (\Delta y)^2}$$

where Δx and Δy are the horizontal and vertical displacements of the jet centerline between computational steps *i* and *i+1* up to the local maximum rise. These displacements are obtained from the columns labeled *Depth* (for the vertical *y*-displacements) and *x-posn* (for the horizontal *x*-displacements).

The computed lengths are 18.9 ft and 16.4 ft respectively.

3. Compute the centerline Kolmogorov scale at the terminal rise height from Eq. 22:

$$\eta_c = 0.24\chi \,\mathrm{Re}^{-3/4}$$
$$= 0.24\times 18.9\times\left(9.2\times 10^5\right)^{-3/4} = 1.5\times 10^{-4}\ \mathrm{ft} = 0.047\ \mathrm{mm}$$

4. Compute entrained flow from Eq. 36:

$$Q_e = nQ_j\left(S_{ta}-1\right)$$
$$= 9\times 10.3\left(6.71-1\right) = 529\ \mathrm{cfs} = 342\ \mathrm{mgd}$$

5. Compute the area of the BMZ (see Figure 2):

$$A_{BMZ} = 2rL + \pi r^2$$
$$= 2\times 28.8\times 192 + \pi\times 28.8^2$$
$$= 13{,}660\ \mathrm{ft}^2 = 0.31\ \mathrm{acre}$$

(For a single rosette diffuser, L would be zero and the radius r would be the radial distance from the riser center to the port openings plus the impact distance.)

Table 4 summarizes the results.

Table 4. Summary of Entrainment, Kolmogorov Scales, and BMZ Areas for Trial Case

Parameter	Salinity requirement met at:	
	Impact point	End of near field
Number of ports, *n*	9	5
Port diameter, *d*	1.13 ft	1.74 ft
Jet velocity, *u*	10.3 ft/s	7.8 ft/s
Froude number, *F*	10.6	6.6
Reynolds number, $\mathrm{Re} = ud/\nu$	9.2×10^5	1.1×10^6
Trajectory length to top, χ	18.9 ft	16.4 ft
UM3 dilution at top, S_{ta}	6.71	4.22
Entrained volume to top, Q_e	529 ft^3/s = 342 mgd	299 ft^3/s = 193 mgd
Centerline Kolmogorov scale at top, η_c (Eq. 22)	1.53×10^{-4} ft = 0.047 mm	1.16×10^{-4} ft 0.035 mm
Area of BMZ	13,660 ft^2 = 0.31 acre	52,270 ft^2 = 1.20 acre

Meeting the salinity requirement at the end of the near field results in fewer ports, a shorter diffuser, lower jet velocity, lower entrainment, but a much larger BMZ. Deciding between the designs will be a policy decision, that, in addition to being a policy call by Water Boards staff, will involve project and site-specific factors.

The Kolmogorov scale at the jet top (i.e., 0.047 mm) is much less than one mm. This is expected to be the usual case for a brine diffuser, but if it is less than one mm at the top, the entrainment calculation can be terminated where the Kolmogorov scale falls to one mm.

5.5 Summary of Diffuser Analysis Procedures

The following section provides a narrative summary of the steps proposed for analysis of (1) entrained volumes exposed to shear forces, and (2) BMZ dilution ratios.

5.5.1 Brine Mixing Zone Analysis Procedures

The purpose of this procedure is to identify the level of dilution, and the associated location within the nearfield mixing zone where that level of mixing may occur. It assumes that the analyst has been provided with a diffuser design for which a mixing zone must be analyzed.

Note that UM3 (preferred) and other models can be used to model brine discharges up to the maximum rise height of the jet trajectory. For dilutions at the seafloor impact location and end-of-nearfield, use the appropriate empirical equations from Section 3.2 of this report.

1. Identify the type of diffuser and reference Section 3.2.

2. Estimate the dilution (S_m) needed to comply with brine receiving water limitation using Equation 37, replacing the numbers with those appropriate for the project.

3. Using acceptable modeling performed for the discharge, identify the location where the dilution identified in step 2 is achieved.
    a. If this dilution is achieved before jet impact on the seabed, then this location is the end of the BMZ (if less than 100 m).
    b. If not, proceed to step 4.

4. Using the empirical equations associated with the diffuser-type identified in step 1, compute the impact and nearfield dilutions and their locations.

a. If the required dilution is met prior to the impact or nearfield locations, use interpolation to find where the required dilution is met.
b. If the required level is not met at the end of the nearfield, evaluate whether the diffuser meets requirements for Best Available Diffuser Design (See Section 5.2) and determine whether an alternative diffuser design may be more appropriate.

5.5.2 Shear Entrained Volume Step-by-step Procedure

The purpose of this procedure is to identify the volume of entrained flow exposed to potentially lethal shearing forces. It assumes that the analyst has been provided with a diffuser design for which entrained volumes (*Qe*) must be estimated.

1. Identify the type of diffuser and collect any modeling (e.g., UM3 modeling) of the diffuser submitted by the diffuser owner. If modeling has not been completed, the analyst should perform UM3 modeling of the diffuser.

2. Using Equation 22, compute the travel distance where the Kolmogorov-scale length equals 1 mm.
   a. If the distance is beyond the jet maximum rise, your shear entrainment dilution is the average dilution (S_{ta}) at the maximum rise.
   b. If the distance is less than the jet maximum rise, your shear entrainment dilution is the average jet dilution at the trajectory location where the Kolmogorov scale equals 1 mm.

3. Convert shear entrainment dilution to the entrained volume rate by multiplying the entrainment dilution by the total discharge flow, Eq. 36.

REFERENCES

Abessi, O., and Roberts, P. J. W. (2014). "Multiport Diffusers for Dense Discharges." *J. Hydraul. Eng.*, 140(8) http://dx.doi.org/10.1061/(ASCE)HY.1943-7900.0000882

Abessi, O., and Roberts, P. J. W. (2015). "Effect of nozzle orientation on dense jets in stagnant environments." J. Hydraul. Eng., 141(8).

Abessi, O., and Roberts, P. J. W. (2017). "Multiport Diffusers for Dense Discharges in Flowing Ambient Water." J. Hydraul. Eng., 143(6).

Abessi, O., Roberts, P. J. W., and Ghandi, V. (2016). "Rosette Diffusers for Dense Effluents." J. Hydraul. Eng., 143(4) 10.1061/(ASCE)HY.1943-7900.0001268

Baumgartner, D. J., Frick, W. E., and Roberts, P. J. W. (1994). "Dilution Models for Effluent Discharges (Third Edition)." U.S. Environmental Protection Agency, Office of Research and Development,.EPA/600/R-94/086

Doneker, R. L., and Jirka, G. H. (1999). "Discussion of mixing of inclined dense jets" by Roberts, P. J. W., Ferrier, A., and Daviero, G." (1997)." J. Hydraul. Eng., 125(3), 317–319.

Fischer, H. B., List, E. J., Koh, R. C. Y., Imberger, J., and Brooks, N. H. (1979). Mixing in Inland and Coastal Waters, Academic Press, New York.

Foster, M.S., Cailliet, G.M., Callaway, J., Vetter, K.M., Raimondi, P., Roberts, P.J.W. (2013). "Desalination Plant Entrainment Impacts and Mitigation." Science Advisory Panel Final Report submitted to Water Resources Control Board, California. 9 October 2013. www.waterboards.ca.gov/water_issues/programs/ocean/desalination/docs/erp_final.pdf

Frick, W. E., Roberts, P. J. W., Davis, L. R., Keyes, J., Baumgartner, D. J., and George, K. P. (2003). "Dilution Models for Effluent Discharges, 4th Edition (Visual Plumes)." U.S. Environmental Protection Agency, Environmental Research Division, NERL, Standards and Applied Science Division, Office of Science and Technology,

Frick, W. E. (2004). "Visual Plumes mixing zone modeling software." Environmental Modelling & Software, 19, 645-654.

Frick, W., Ahmed, A., George, K., Laputz, A., Pelletie, G., and Roberts, P. (2010). "On Visual Plumes and Associated Applications." MWWD 2010 6th International Conference on Marine Waste Water Discharges and Coastal Environment, C. Avanzini, ed. Langkawi, Malaysia.

Frick, W. E., and Roberts, P. J. W. (2016). "Visual Plumes 2016: An Updated Public-Domain Plume Model Suite." Proc., International Symposium on Outfall Systems, ISOS2016, IWA. 10 - 13 May 2016.

Marti, C. L., Antenucci, J. P., Luketina, D., Okely, P., and Imberger, J. (2011). "Near-Field Dilution Characteristics of a Negatively Buoyant Hypersaline Jet Generated by a Desalination Plant." *J. Hydraul. Eng.*, 137(1), 57-65 10.1061/(ASCE)HY.1943-7900.0000275

Miller, B. M., Cunningham, I. L., and Timms, W. A. (2007). "Physical modeling of the seawater concentrate diffusers for the Sydney desalination study." The University of

New South Wales, School of Civil and Environmental Engineering, Water Research Laboratory. WRL Technical Report 2007/04

Palomar, P., Lara, J. L., and Losada, I. J. (2012). "Near field brine discharge modeling Part 2: Validation of commercial tools." Desalination, 290(0), 28-42.

Roberts, P. J. W., Ferrier, A., and Daviero, G. J. (1997). "Mixing in Inclined Dense Jets." *J. Hydraul. Eng*., 123(8), 693-699.

Roberts, P. J. W., and Snyder, W. H. (1993). "Hydraulic Model Study for the Boston Outfall. I: Riser Configuration." J. Hydraul. Eng., 119(9), 970-987.

Roberts, P. J. W., Salas, H. J., Reiff, F. M., Libhaber, M., Labbe, A., and Thomson, J. C. (2010). Marine Wastewater Outfalls and Treatment Systems, International Water Association, London.

Roberts, P. J. W. (2016). "Modeling Brine Disposal into Monterey Bay." Atlanta, Georgia. Final Report, Prepared for ESA | Environmental Science Associates San Francisco, California. July 6, 2016

State Water Board (2016). "Water Quality Control Plan Ocean Waters of California." State Water Resources Control Board, California Environmental Protection Agency, Sacramento, California, Adopted May 6, 2015, Effective January 28, 2016.

Tarrade, L., and Miller, B. M. (2010). "Physical modeling of the Victorian desalination plant outfall." The University of New South Wales, School of Civil and Environmental Engineering, Water Research Laboratory. WRL Technical Report 2010/06.

USEPA (1991). "Technical Support Document for Water Quality-Based Toxics Control." U.S. EPA Office of Water.EPA 505/2-90-001

USEPA (1994). "Amended Section 301(h) Technical Support Document." Oceans and Coastal Protection Division, Office of Wetlands, Oceans and Watersheds, United States Environmental Protection Agency.EPA 842-B-94-007

Walter, R. K., Squibb, M. E., Woodson, C. B., Koseff, J. R., and Monismith, S. G. (2014). "Stratified turbulence in the nearshore coastal ocean: Dynamics and evolution in the presence of internal bores." Journal of Geophysical Research: Oceans, 10.1002/2014jc010396, 119(12), 8709-8730.

Webster, D. R., Roberts, P. J. W., and Ra'ad, L. (2001). "Simultaneous DPTV/PLIF measurements of a turbulent jet." Expts. Fluids, 30, 65-72

Wygnanski, I., and Fiedler, H. E. (1969). "Some Measurements in the Self-Preserving Jet." J. Fluid Mech., 38(3), 577-612

APPENDIX A. TURBULENCE EFFECTS ON ORGANISMS

This section reviews the literature on the effects of turbulence and shear stress on aquatic organisms. It is based on Foster et al. (2013).

Most of the data are from laboratory experiments that exposed various types of larvae to controlled levels of laminar shear stress in a Couette cell, or to turbulence generated by either an oscillating grid, shaken flasks, bubble plumes, or other mechanisms. These devices create environments that are very different from the types of water movement experienced by larvae in nature. For example, laboratory experiments typically aspire to homogenous turbulence, while turbulence in nature or in diffuser jets is not homogenous. Furthermore, the laboratory experiments typically involve exposing the larvae to some level of turbulent intensity for times usually much longer than the expected duration of exposure in diffuser jets. For example, many of the experiments expose larval or adult organisms to shear stress for an hour per day, as opposed to seconds in the jet. While the Nietzel et al. (2004) study looks at short-term exposure of juvenile fish forced to enter a submerged jet, the velocities and shear strain rates are much higher than those relevant for the diffuser type outfall considered here. In the one field assessment reported by Jessopp (2007), the velocities measured, combined with distances (from Google Earth), indicate the exposure to damaging turbulence in the natural tidal rapids investigated is probably on the order of minutes rather than seconds.

The effects of turbulence vary with species and with size of organism. Small scale (< 1 cm) turbulence can accelerate development rates of marine copepods in microcosms (Oviatt 1981; Alcaraz et al. 1988; Saiz and Alcaraz 1991), increase excretion rates (Saiz and Alcaraz 1992a), and modify copepod activity and behavior (Costello et al. 1990; Saiz and Alcaraz 1992b). However, this enhancement of highly expensive motor activity (i.e. higher frequency of feeding bouts and escape reactions, Marrasé et al. 1990; Saiz and Alcaraz 1992b) can increase copepod metabolic rates. The increased energy expenditures can lead to decreased growth rates, even if development is accelerated (Peters and Marrasé 2000). Other effects (at higher energy dissipation rates) include abnormal fertilization and development (Mead and Denny 1995) and increases in mortality (Rehmann et al. 2003; Maldonaldo and Lutz 2011).

In general, turbulent eddies that are much bigger than the larvae merely transport them, without affecting them adversely. Smaller turbulent eddies could increase mortality, since velocity gradients exist on a scale small enough to affect the larvae (Rehmann 2003). Thus, very small gametes probably escape damage, as do perhaps large organisms with tough integument. Fish and other larvae on the mm/cm scale may well be susceptible to damage. However, the probability of

exposure to the smallest-scaled, most energetic turbulence at the jet centerline is likely to be low.

It is important to be aware that temperature, oxygen content, salinity, alkalinity, and vertical mixing are all factors that affect mortality in addition to the effects of turbulence (Eilav et al. 2002, Danoun 2007). None of the experiments considered any, let alone all, of these additional, possibly synergistic, sources of mortality. It would be advisable to invest in experiments that more closely reproduce the likely experience of entrained larvae. This would help the community to more accurately assess probable outcomes.

Organism	Shear stress or turbulence	Method of generating shear/turbulence	Magnitude of critical shear/turbulence	Effect	Reference	Additional notes
Sea urchin *S. purpuratus* larvae (3 day; prism)	Laminar shear	Couette flow[1], short term (30 min)	No deleterious effect with $\varepsilon \leq 1$ cm^2/s^3	Change in prey encounter rate	Maldonaldo and Latz (2011)	Negative effect could be due to erosion of hydromechanical signal, or if local velocity faster than catch speed, reaction time. Mortality was 19% for the 0.1 cm^2/s^3, 22% for the 0.4 cm^2/s^3, and 53% for the 1 cm^2/s^{3}flow treatments compared to 5% for the still control.
		Couette flow Long term (8 days of 12 h on, 12 h off)	$\varepsilon < 0.1$ cm^2/s^3	Excessive mortality		
Sea urchin *L. pictus larvae* (3 day, 4 arm pluteus)	Laminar shear	Couette flow[1],short term (30 min)	No deleterious effect with $\varepsilon \leq 1$ cm^2/s^3	Change in prey encounter rate	Maldonaldo and Latz (2011)	
		Couette flow Long term (8 days of 12 h on, 12 h off)	No deleterious effect with $\varepsilon \leq 1$ cm^2/s^3	Some mortality, but not much		
Sea urchin *S. purpuratus*	Shear stress	Couette flow (short term: 2 min)	No deleterious effect with $\varepsilon < 200$ cm^2/s^3	Fertilization and development to blastula	Mead and Denny (1995), Denny, Nelson and Mead (2002)	
Zebra mussel *Dreissena polymorpha* veliger	Turbulence	Bubble plume for 24 hours, then 24 feed before mortality measured	Mortality increases when d* > 0.9 (eddy similar in size to larva (no sig eff when d*<0.9)	Mortality	Rehmann et al. (2003)	
dinoflagellate *Alexandrium fundyense*	Laminar shear	Couette flow for 1-24 hours/day	Shear stress $\tau = 0.003$ N/m^2 ; $\varepsilon = 10^{-5}$ cm^2/s^3 ; only 1 level	Growth rate decreased when exposed to τ for more than 2 hours/ day	Juhl et al. (2001)	Growth rate = 0 when shear 12 h/d; negative when 16-24 h/day
dinoflagellate *Alexandrium fundyense*	Laminar shear and turbulence	Couette flow 1 h/d 5–8 d and shaken flasks	Shear stress $\tau = 0.004$ N/m^2 (not quantified for shaken flasks	Growth rate decreased in both	Juhl et al. 2000	Most sensitive last hour of dark phase, under lower light conditions
dinoflagellate *Lingulodiniu m polyedrum.*	Shear (steady and unsteady)	Couette flow; constant or changing speeds/direction; 2 h/d (change ev 2 min)	smallest $\varepsilon = 0.04$ cm^2/s^3; all had effect (very very high)	Growth rate decreased in all cases; often catastrophically (near 100%)	Latz et al. 2009	Unsteady flow had more of an effect than steady, even when mean was lower; possible mechanism: mechanical energy of the flow alters membrane biophysical properties, activates signal transduction pathway involving GTP, [ca2+]I, poss. Also involves cyclin-dep kinases, as in endothelial cells

Organism	Shear stress or turbulence	Method of generating shear/turbulence	Magnitude of critical shear/turbulence	Effect	Reference	Additional notes
Copepod *Acartia tonsa*	Turbulence	model	Starts dropping at $\varepsilon = 10^{-3}$ cm^2/s^3	Decrease in prey capture success	Kiørboe and Saiz 1995	Copepods that set up feeding currents are largely independent of ambient fluid velocity for prey encounters, while ambush-preying copepods can benefit substantially
Copepod *Acartia tonsa*	Turbulence	Oscillating grid			Saiz & Kiørboe 1995	
Herring larvae	Turbulence	model	Starts dropping at $\varepsilon = 10^{-3}$ cm^2/s^3	Decrease in prey capture success	Kiørboe and Saiz 1995	
Cod larvae	Turbulence	model	Starts dropping at $\varepsilon = 10^{-5}$ cm^2/s^3	Decrease in prey capture success	Kiørboe and Saiz 1995	
Cod *Gadus morhua* (5-6 mm)	Turbulence	Oscillating grid; observations start after 10 min shaking	$\varepsilon = 7.4 \times 10^{-4}$ cm^2/s^3)	Increase in "attack position rate" at all concentrations	MacKenzie and Kiørboe 1995	Cod benefit more from turbulence (pause-travel)
Cod *Gadus morhua* (8.7-12.3 mm)	Turbulence -more intermitten t	Oscillating grid, observations start after a few min shaking	$\varepsilon = .2, 2 \times 10^{-4}$ cm^2/s^3)	While encounter rate up, pursuit success down	MacKenzie and Kiorboe 2000	Decrease in pursuit success at higher ε; general downward trend with increased relative velocity; smaller fish larvae affected more
Herring *Clupea harengus* (8-9 mm)	Turbulence	Oscillating grid; observations start after 10 min shaking	$\varepsilon = 7.4 \times 10^{-4}$ cm^2/s^3)	Increase in "attach position rate" only at low concentrations; very messy data	MacKenzie and Kiorboe 1995	Herring benefit less (cruise)
Juvenile rainbow trout and steelhead *Oncorhynchus mykiss,* Chinook salmon *O. tshawytscha,* American shad *Alosa sapidissima*	Shear stress	Forced entry directly into submerged jet in flume having exit velocities of 0 to 21.3 m/s	No effect at 168/s 341/s; LC-10 estimated at 495/s	Torn opercula, missing eyes	Nietzel et al. 2004	LC-10 =affects 10% of population of juvenile fish 83-232 mm fork length
Water flea *Daphnia pulex*	Turbulence	Vibrating 0.5 cm grid	$\varepsilon = 0.05$ cm^2/s^3 (as compared to calm)	Heart rate increased 5- 27%	Alvarez et al. 1994	HR reflects increase in metabolic rate?
Copepod *Calanus gracilis*	Turbulence	Vibrating 0.5 cm grid	$\varepsilon = 0.05$ cm^2/s^3 (as compared to calm)	Heart rate increased 93%	Alvarez et al. 1994	Other species too including crab larvae (increase HR 9%)
Copepod *Acartia tonsa*	Turbulence	Oscillating grid	$\varepsilon = 0.001$ cm^2/s^3 (as compared to calm)	Decreases predator sensing ability	Gilbert and Buskey 2005	

Organism	Shear stress or turbulence	Method of generating shear/turbulence	Magnitude of critical shear/turbulence	Effect	Reference	Additional notes
Copepod *Acartia tonsa*	Turbulence (field)	Boat wake (field); plankton tow inside/ outside wake	ε = 310 cm^2/s^3 at a distance of 50 propeller diam. behind 20 mm diam, scale-model boat propeller running at 3000 rpm	More dead inside wake (5- 25% increase, over 2-12% background)	Bickel et al. 2011	Stain with neutral red
Copepod *Acartia tonsa*		Mini stirrer with paddles (lab)	ε = 0, 0.035, 1.31, 2.24 cm^2/s^3		Bickel et al. 2011	ε = 0.035 cm^2/s^3 did not show negative effect
Various	Turbulence (field)	Rapids (samples collected above and below rapids	ε = 3-742 cm^2/s^3	Effects dep on species: sign. mortality in *Littorina littorea*, *Mytilus edulis*, and *Aporrhais pespelicant*	Jessop 2007	*Mytilus membranipora*, *Electra pilosa*, polychaete trochophores and *Lamellaria perspicua* had zero mortality

ε = energy dissipation rate (cm^2/s^3)

Couette flow: two concentric cylinders, outer one rotates shearing volume of fluid between cylinders at known rate

Bibliography – Biological Effects

Alcarez, M., E. Saiz, and A. Calbet. (1994). Small-scale turbulence and zooplankton metabolism: Effects of turbulence on heartbeat rates of planktonic crustaceans. Limnol. Oceanogr., 39(6), 1994, 1465-1470

Bickel, S. L., J. D. M. Hammond, & K. W. Tang (2011). Boat-generated turbulence as a potential source of mortality among copepods. Journal of Experimental Marine Biology and Ecology 401: 105–109

Bruton, M. N. (1985). The effects of suspensoids on fish. *Hydrobiologia* 125: 221-241.

Chesney, E. J., Jr (1989). Estimating the food requirements of striped bass larvae *Morone saxatilis:* effects of light, turbidity and turbulence. Mar. Ecol. Prog. Ser. Vol. 53: 191-200.

Dauvin, J.-C. and J. J. Dodson (1990) Relationship between feeding incidence and vertical and longitudinal distribution of rainbow trout larvae (*Osmerus mordax*) in a turbid, well-mixed estuary. Mar. Ecol. Prog. Ser. Vol. 60: 1-12.

Einav, R., K. Hamssib, D. Periy (2002). The footprint of the desalination processes on the environment. Desalination 152 (2002) 141-154

Evans, M. S. (1981). Distribution of zooplankton populations within and adjacent to a thermal plume. Can. J. Fish. Aquat. Sci. 38: 441-448.

Huang, S., N. Voutchkov, S. C. Jiang (2013). Investigation of environmental influences on membrane biofouling in a Southern California desalination pilot plant. Desalination 319: 1–9

Jessopp, M. J. (2007) The quick and the dead: larval mortality due to turbulent tidal transport. J. Mar. Biol. Ass. U.K. 87, 675-680.

Jones, I. S. F. & Y. Toba [EDS.]. (2001) Wind stress over the ocean. Cambridge Univ. Press.

Juhl, A. R., V. Velasquez, M. I. Latz (2000) Effect of growth conditions on flow-induced inhibition of population growth of a red-tide dinoflagellate. Limnol Oceanogr 45:905–915

Juhl, A. R., V. L. Trainer, M. I. Latz (2001) Effect of fluid shear and irradiance on population growth and cellular toxin content of the dinoflagellate *Alexandrium fundyense*. Limnol Oceanogr 46: 758–764

Kiørboe, T., E. Saiz (1995) Planktivorous feeding in calm and turbulent environments, with emphasis on copepods. Mar Ecol Prog Ser 122: 135–145.

Latz, M.I., J. Allen, S. Sarkar, J. Rohr (2009) Effect of fully characterized unsteady flow on population growth of the dinoflagellate *Lingulodinium polyedrum*. Limnol Oceanogr 54:1243–1256.

Lunz, R. G. (1938). Part I. Oyster culture with reference to dredging operations in South Carolina. Part II. The effects of the flooding of the Santee River in April 1936 on oysters in the Cape Romain area of South Carolina. Report to U. S. Engineer Office, Charleston, South Carolina, 1-33.

MacKenzie, B. R. and T. Kiørboe (1995). Encounter rates and swimming behavior of pause-travel and cruise larval fish predators in calm and turbulent laboratory

environments. Limnol. Oceanogr., 40(T), 1995, 1278-1289.

MacKenzie, B. R. and T. Kiørboe (2000). Larval fish feeding and turbulence: A case for the downside. Limnol. Oceanogr., 45(1), 2000, 1–10

Maldonado, E. M. and Latz, M.I. (2011) Species-specific effects of fluid shear on grazing by sea urchin larvae: comparison of experimental results with encounter-model predictions. Mar Ecol Prog Ser 436:119-130

Mead, K. and Denny, M. (1995). Effects of hydrodynamic shear stress on the fertilization and early development of the purple sea urchin, *Strongylocentrotus purpuratus*. *Biol. Bull.* 188: 46-56.

Miner J.G., Stein R.A. (1996) Detection of predators and habitat choice by small bluegills: effects of turbidity and alternative prey. Trans Am Fish Soc 125:97±103.

Peters F, C. Marrasé (2000). Effects of turbulence on plankton: an overview of experimental evidence and some theoretical considerations. Mar. Ecol. Prog. Ser. 205: 291–306.

Rehmann, C. R., J.A. Stoeckel, and D.W. Schneider (2003a). Effect of turbulence on the mortality of zebra mussel veligers. Can. J. Zool. 81: 1063–1069

Roberts, Roberts, P. J. W. (2018). "Brine Diffusers and Shear Mortality: Application to Huntington Beach." Final Report. Prepared for Eastern Research Group, April 2018.

Saiz, E., T. Kiørboe (1995). Predatory and suspension feeding of the copepod Acartia *tonsa* in turbulent environments. Mar. Ecol. Prog. Ser. 122: 147-158

SCCWRP (2012), Management of Brine Discharges to Coastal Waters Recommendations of a Science Advisory Panel," submitted at the request of the State Water Resources Control Board by the Southern California Coastal Water Research Project, Costa Mesa, CA, Technical Report 694, March 2012

Vinyard, G. L. and W. J. O'Brien (1976) Effects of Light and Turbidity on the Reactive Distance of Bluegill (*Lepomism acrochirus*) J. Fish. Res. Board Can. 13:2845-2849.

Zhang, C., Xu, M., Wang, Z., Liu, W., and Yu, D. (2017). "Experimental study on the effect of turbulence in pipelines on the mortality of Limnoperna fortunei veligers." Ecological Engineering, 109(Part A), 101-118 https://doi.org/10.1016/j.ecoleng.2017.08.024.

APPENDIX B. UM3 SIMULATIONS

These are the UM3 outputs for the diffuser cases in Tables 3 and 4.

Contents of the memo box (may not be current and must be updated manually)
Project "C:\Plumes17\Shear mortality\Impact point" memo
memo

Model configuration items checked:
  Channel width (m) 100
Start case for graphs 1
Max detailed graphs 10 (limits plots that can overflow memory)
 Elevation Projection Plane (deg) 0
Shore vector (m,deg) not checked
 Bacteria model : Mancini (1978) coliform model
 PDS sfc. model heat transfer : Medium
 Equation of State : S, T
 Similarity Profile : Default profile (k=2.0, ...)
 Diffuser port contraction coefficient 1
 Light absorption coefficient 0.16
 Farfield increment (m) 200
 UM3 aspiration coefficient 0.1
  Output file: text output tab
  Output each ?? steps 10
  Maximum dilution reported 100
 Text output format : Standard
 Max vertical reversals : to max rise or fall

/ UM3. 1/5/2018 2:58:02 PM
Case 1; ambient file C:\Plumes17\Shear mortality\Impact point.001.db; Diffuser table record 1:

Ambient Table:

Depth	Amb-cur	Amb-dir	Amb-sal	Amb-tem	Amb-pol	Decay	Far-spd	Far-dir	Disprsn	Density
m	m/s	deg	psu	C	kg/kg	s-1	m/s	deg	m0.67/s2	sigma-T
0.0	0.0	0.0	34.00	20.00	0.0	0.0	-	-	0.0	24.02299
12.19	0.0	0.0	34.00	20.00	0.0	0.0	-	-	0.0	24.02299

Diffuser table:

P-diaVer	angl	H-Angle	SourceX	SourceY	Ports	Spacing	MZ-dis	Isoplth	P-depth	Ttl-flo	Eff-sal	Temp	Polutnt
(ft)	(deg)	(deg)	(m)	(m)	()	(ft)	(ft)	(concent)	(ft)	(ft3/s)	(psu)	(C)	(ppm)
1.1300	60.000	0.0	0.0	0.0	9.0000	24.000	328.08	0.0	30.000	92.800	68.000	20.000	1000.0

Simulation:
Froude No: -10.74; Strat No: 0.0000; Spcg No: 21.24; k: 3.13E+5; eff den (sigmaT) 50.49684; eff vel 3.134(m/s);
Current is very small, flow regime may be transient.

Step	Depth (ft)	P-dia (ft)	P-speed (m/s)	Dilutn ()	x-posn (ft)	Iso dia (m)	
0	30.00	1.130	3.134	1.000	0.0	0.3444;	
10	29.48	1.357	2.583	1.213	0.299	0.4136;	
20	28.83	1.663	2.104	1.485	0.681	0.5069;	
30	28.03	2.040	1.708	1.815	1.153	0.6219;	
40	27.06	2.509	1.379	2.219	1.738	0.7649;	
50	25.87	3.099	1.104	2.710	2.473	0.9445;	
60	24.42	3.852	0.871	3.309	3.410	1.1740;	
70	22.70	4.827	0.674	4.021	4.610	1.4713;	
80	21.34	5.705	0.554	4.583	5.657	1.7390;	
90	20.37	6.408	0.480	4.988	6.489	1.9532;	
100	19.64	6.998	0.428	5.298	7.181	2.1329;	
110	19.08	7.506	0.390	5.543	7.773	2.2880;	
120	18.63	7.954	0.361	5.743	8.292	2.4243;	
130	18.27	8.352	0.337	5.911	8.755	2.5458;	
140	17.98	8.710	0.318	6.054	9.173	2.6549;	
147	17.80	8.940	0.306	6.143	9.444	2.7250;	begin overlap;
150	17.74	9.033	0.302	6.178	9.555	2.7532;	
160	17.54	9.309	0.289	6.275	9.908	2.8376;	
170	17.38	9.546	0.278	6.353	10.24	2.9096;	
180	17.24	9.750	0.269	6.417	10.55	2.9717;	
190	17.13	9.927	0.262	6.470	10.85	3.0257;	
200	17.04	10.08	0.256	6.516	11.13	3.0724;	
210	16.97	10.21	0.251	6.557	11.40	3.1129;	
220	16.91	10.33	0.247	6.594	11.67	3.1476;	
230	16.87	10.42	0.244	6.628	11.93	3.1770;	
240	16.84	10.50	0.241	6.659	12.18	3.2015;	
250	16.83	10.57	0.240	6.690	12.43	3.2213;	
258	16.83	10.61	0.239	6.713	12.63	3.2340;	local maximum rise or fall;
260	16.83	10.62	0.238	6.719	12.68	3.2368;	
270	16.84	10.66	0.238	6.748	12.93	3.2480;	
280	16.86	10.68	0.238	6.778	13.17	3.2552;	
290	16.90	10.69	0.238	6.808	13.42	3.2586;	
300	16.94	10.69	0.240	6.840	13.68	3.2585;	
310	17.01	10.68	0.241	6.873	13.93	3.2549;	

320	17.09	10.66	0.244	6.909	14.20	3.2482;	
330	17.18	10.63	0.247	6.949	14.46	3.2387;	
340	17.30	10.59	0.250	6.994	14.74	3.2267;	
350	17.43	10.54	0.254	7.045	15.03	3.2128;	
360	17.59	10.49	0.259	7.104	15.33	3.1975;	
370	17.78	10.44	0.264	7.174	15.65	3.1817;	
380	18.00	10.39	0.270	7.259	15.98	3.1664;	
390	18.27	10.34	0.276	7.362	16.33	3.1531;	
400	18.57	10.31	0.282	7.491	16.70	3.1438;	
404	18.71	10.31	0.285	7.552	16.85	3.1416;	end overlap;
410	18.94	10.30	0.289	7.649	17.10	3.1388;	
420	19.37	10.28	0.297	7.831	17.52	3.1349;	
430	19.88	10.28	0.305	8.044	17.98	3.1333;	
440	20.50	10.29	0.315	8.297	18.49	3.1356;	
450	21.25	10.31	0.325	8.602	19.04	3.1440;	
460	22.17	10.37	0.335	8.976	19.65	3.1615;	
470	23.31	10.47	0.346	9.446	20.32	3.1921;	
480	24.76	10.64	0.357	10.05	21.08	3.2417;	
490	26.61	10.89	0.367	10.84	21.95	3.3185;	
500	29.03	11.27	0.376	11.91	22.94	3.4349;	
510	32.28	11.84	0.383	13.41	24.08	3.6099;	
520	36.75	12.71	0.387	15.61	25.41	3.8743;	
523	38.43	13.05	0.387	16.47	25.86	3.9782;	bottom hit;
530	42.97	14.00	0.385	18.90	26.94	4.2678;	
540	50.17	15.57	0.379	23.04	28.41	4.7473;	
550	58.25	17.39	0.371	28.09	29.78	5.3019;	
560	67.32	19.48	0.360	34.25	31.06	5.9370;	
570	77.52	21.85	0.349	41.75	32.28	6.6599;	
579	87.77	24.26	0.338	49.91	33.33	7.3932;	merging;
580	89.24	24.64	0.338	50.90	33.47	7.5118;	
590	114.4	34.23	0.366	62.06	35.47	10.433;	
600	150.9	41.68	0.398	75.65	37.68	12.704;	
610	195.7	50.18	0.418	92.23	39.76	15.295;	
615	221.8	55.21	0.425	101.8	40.78	16.827;	stop dilution reached;

Horiz plane projections in effluent direction: radius(m): 0.0; CL(m): 12.429
Lmz(m): 12.429
forced entrain 1 0.0 -58.45 16.83 0.038
Rate sec-1 0.0 dy-1 0.0 kt: 0.0 Amb Sal 34.0000
;
2:58:02 PM. amb fills: 4

Diffuser: Impact point.vpp.db | Ambient: C:\Plumes17\Shear mortality\Impact point.001.db | Special Settings | Text Output | Graphical Output

Style

Series

Plane

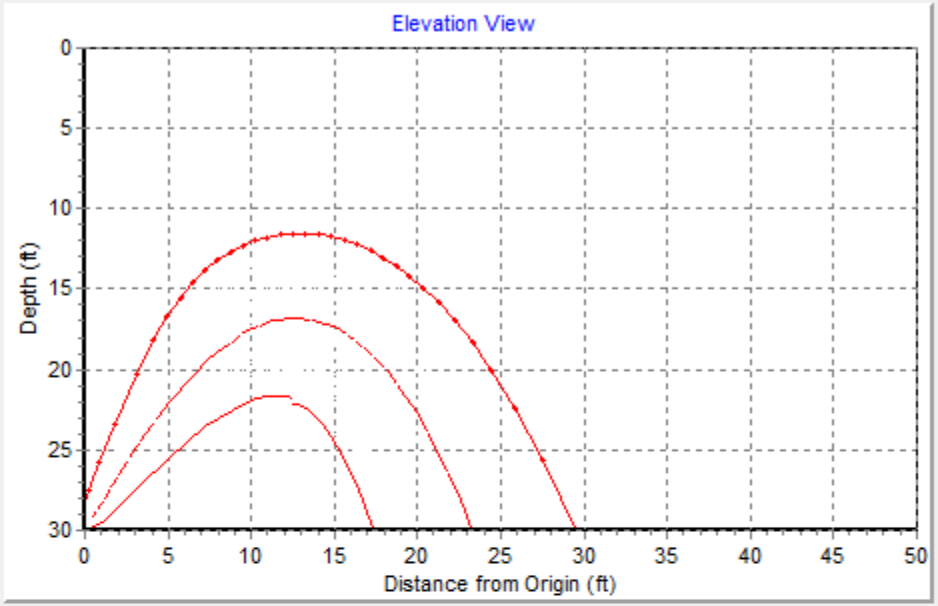

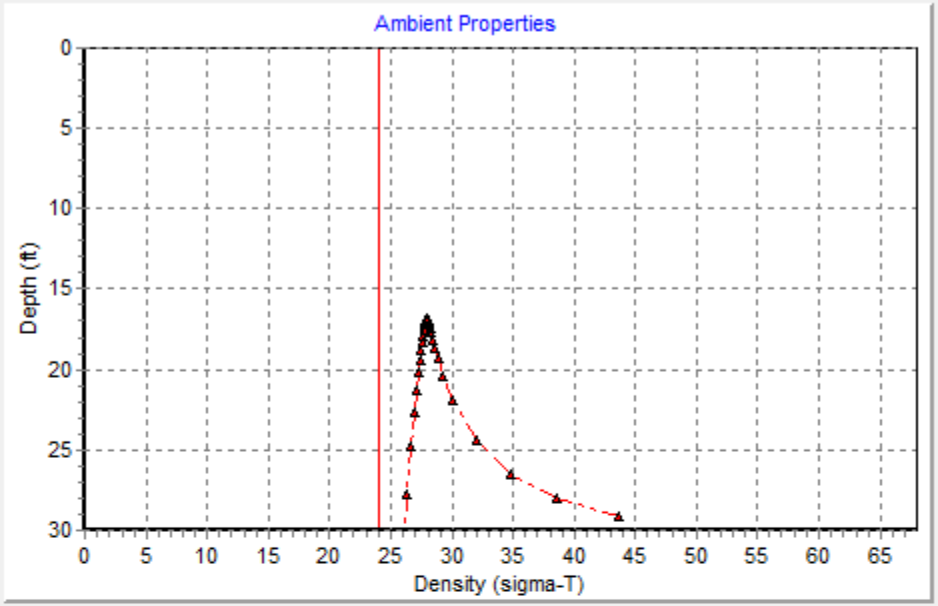

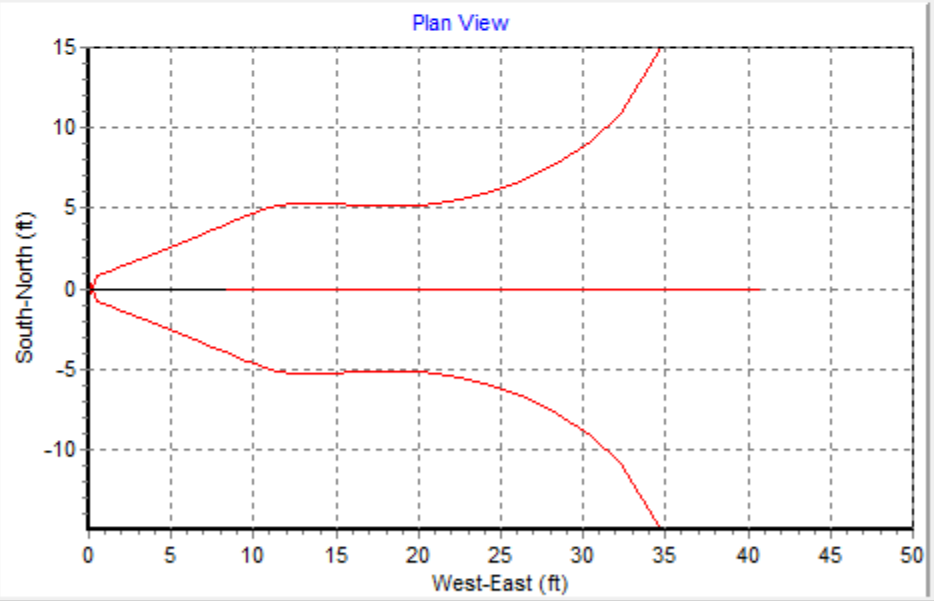

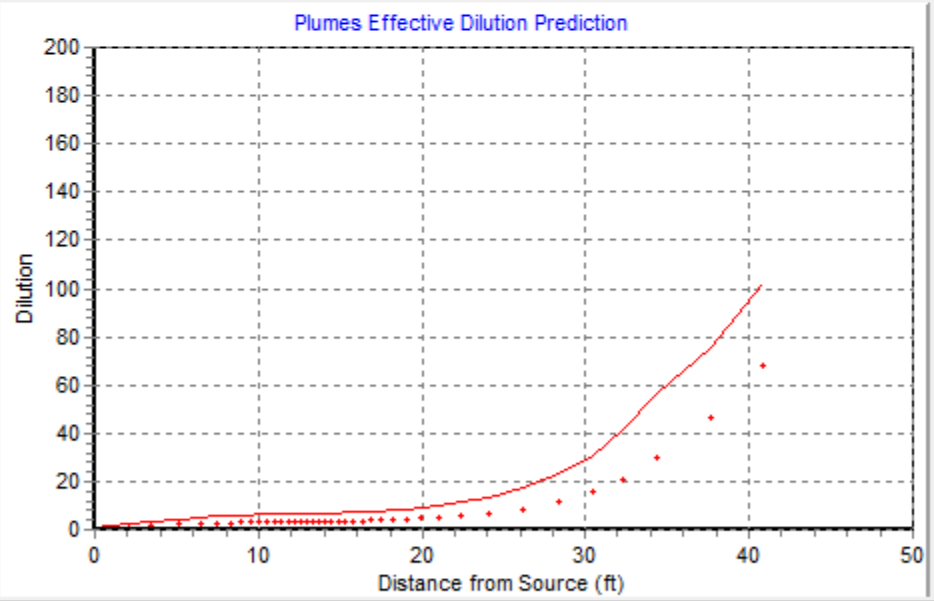

/ UM3. 1/5/2018 3:01:56 PM
Case 1; ambient file C:\Plumes17\Shear mortality\Near field.001.db; Diffuser table record 1:

Ambient Table:

Depth m	Amb-cur m/s	Amb-dir deg	Amb-sal psu	Amb-tem C	Amb-pol kg/kg	Decay s-1	Far-spd m/s	Far-dir deg	Disprsn m0.67/s2	Density sigma-T
0.0	0.0	0.0	34.00	20.00	0.0	0.0	-	-	0.0	24.02299
12.19	0.0	0.0	34.00	20.00	0.0	0.0	-	-	0.0	24.02299

Diffuser table:

P-dia (ft)	Ver angl (deg)	H-Angle (deg)	SourceX (m)	SourceY (m)	Ports ()	Spacing (ft)	MZ-dis (ft)	Isoplth (concent)	P-depth (ft)	Ttl-flo (ft3/s)	Eff-sal (psu)	Temp (C)	Polutnt (ppm)
1.7300	60.000	0.0	0.0	0.0	5.0000	24.000	328.08	0.0	30.000	92.800	68.000	20.000	1000.0

Simulation:
Froude No: -6.666; Strat No: 0.0000; Spcg No: 13.87; k: 2.41E+5; eff den (sigmaT) 50.49684; eff vel 2.407(m/s);
Current is very small, flow regime may be transient.

Step	Depth (ft)	P-dia (ft)	P-speed (m/s)	Dilutn ()	x-posn (ft)	Iso dia (m)	
0	30.00	1.730	2.407	1.000	0.0	0.5273;	
10	29.23	2.073	1.981	1.207	0.445	0.6317;	
20	28.24	2.554	1.596	1.477	1.039	0.7783;	
30	27.02	3.160	1.272	1.806	1.786	0.9633;	
40	25.53	3.942	0.997	2.207	2.746	1.2015;	
50	23.88	4.904	0.777	2.651	3.903	1.4949;	
60	22.69	5.697	0.650	2.973	4.833	1.7364;	
70	21.83	6.340	0.568	3.209	5.582	1.9326;	
80	21.17	6.885	0.510	3.390	6.210	2.0985;	
90	20.66	7.357	0.466	3.535	6.750	2.2426;	
100	20.25	7.774	0.432	3.654	7.226	2.3697;	
110	19.93	8.147	0.405	3.754	7.651	2.4832;	
120	19.66	8.482	0.382	3.839	8.036	2.5854;	
124	19.57	8.607	0.374	3.870	8.180	2.6235;	begin overlap;
130	19.44	8.780	0.364	3.911	8.388	2.6763;	
140	19.26	9.033	0.349	3.967	8.715	2.7534;	
150	19.11	9.250	0.337	4.011	9.021	2.8196;	
160	18.99	9.438	0.326	4.048	9.310	2.8769;	
170	18.89	9.602	0.318	4.079	9.586	2.9266;	
180	18.81	9.743	0.311	4.106	9.850	2.9698;	
190	18.74	9.866	0.305	4.130	10.10	3.0071;	
200	18.69	9.970	0.300	4.151	10.35	3.0390;	
210	18.65	10.06	0.297	4.171	10.59	3.0659;	
220	18.63	10.13	0.294	4.190	10.83	3.0882;	
230	18.61	10.19	0.292	4.208	11.07	3.1061;	
236	18.61	10.22	0.291	4.218	11.20	3.1147;	local maximum rise or fall;
240	18.61	10.24	0.290	4.225	11.30	3.1197;	
250	18.63	10.27	0.290	4.243	11.53	3.1294;	
260	18.65	10.29	0.290	4.260	11.76	3.1352;	
270	18.68	10.29	0.291	4.278	12.00	3.1374;	
280	18.73	10.29	0.293	4.297	12.23	3.1361;	
290	18.79	10.27	0.295	4.317	12.47	3.1315;	
300	18.87	10.25	0.298	4.339	12.72	3.1240;	
310	18.96	10.22	0.302	4.363	12.97	3.1137;	
320	19.07	10.17	0.306	4.390	13.24	3.1010;	
330	19.20	10.13	0.311	4.421	13.51	3.0863;	
340	19.35	10.07	0.317	4.457	13.79	3.0704;	
350	19.53	10.02	0.324	4.500	14.09	3.0538;	
360	19.74	9.966	0.331	4.552	14.40	3.0377;	
370	19.99	9.920	0.339	4.616	14.73	3.0236;	
380	20.29	9.886	0.347	4.696	15.08	3.0132;	
384	20.42	9.877	0.350	4.733	15.23	3.0106;	end overlap;
390	20.64	9.866	0.356	4.794	15.46	3.0071;	
400	21.05	9.850	0.365	4.907	15.87	3.0024;	
410	21.54	9.842	0.376	5.041	16.30	2.9998;	
420	22.14	9.846	0.387	5.199	16.78	3.0011;	
430	22.86	9.870	0.400	5.391	17.31	3.0083;	
440	23.75	9.922	0.413	5.627	17.89	3.0244;	
450	24.86	10.02	0.427	5.924	18.54	3.0533;	
460	26.26	10.17	0.440	6.306	19.27	3.1009;	
470	28.06	10.42	0.453	6.809	20.09	3.1752;	
480	30.42	10.79	0.465	7.494	21.04	3.2887;	
490	33.59	11.35	0.473	8.458	22.14	3.4602;	
500	37.99	12.21	0.478	9.878	23.43	3.7208;	
501	38.53	12.31	0.478	10.06	23.57	3.7535;	bottom hit;
510	44.05	13.47	0.475	11.99	24.89	4.1051;	
520	50.99	14.99	0.468	14.62	26.27	4.5680;	
530	58.78	16.74	0.457	17.82	27.57	5.1031;	

```
 540     67.52    18.75    0.444    21.73    28.78    5.7154;
 550     77.34    21.04    0.430    26.50    29.93    6.4122;
 560     88.38    23.63    0.415    32.31    31.03    7.2023;
 562     90.75    24.19    0.412    33.61    31.24    7.3724; merging;
 570     107.7    30.86    0.431    39.39    32.59    9.4070;
 580     141.6    39.38    0.473    48.02    34.68    12.004;
 590     183.7    47.27    0.502    58.54    36.66    14.408;
 600     235.1    57.19    0.520    71.37    38.55    17.433;
 610     297.9    69.42    0.533    87.00    40.40    21.160;
 618     358.1    81.15    0.540    101.9    41.85    24.736; stop dilution reached;
Horiz plane projections in effluent direction: radius(m):      0.0; CL(m):   12.756
Lmz(m):   12.756
forced entrain      1     0.0  -100.0   24.74  0.0229
Rate sec-1          0.0 dy-1          0.0  kt:          0.0 Amb Sal      34.0000
 ;
3:01:56 PM. amb fills: 4
```

Diffuser: Near field.vpp.db | Ambient: C:\Plumes17\Shear mortality\Near field.001.db | Special Settings | Text Output | Graphical Output

Style

Series
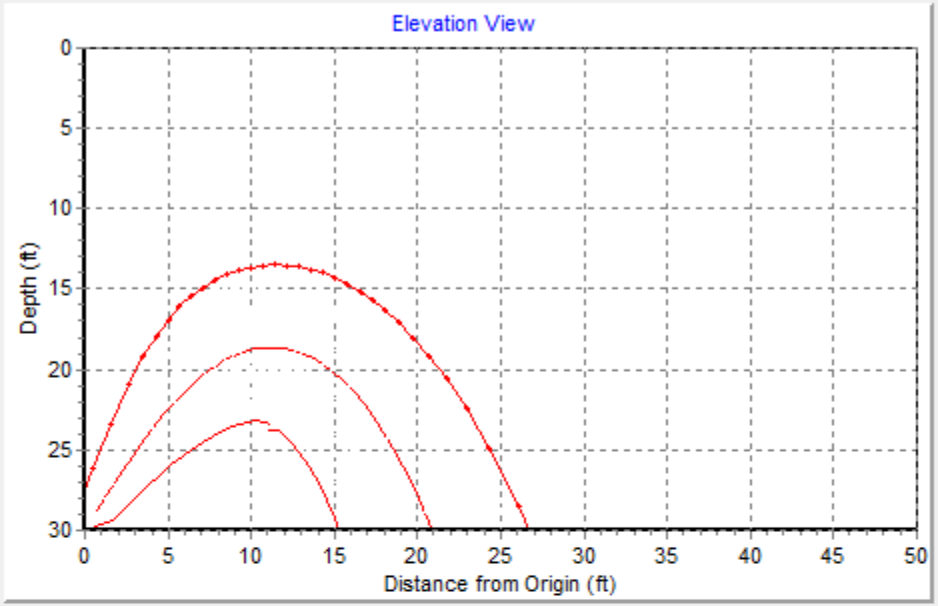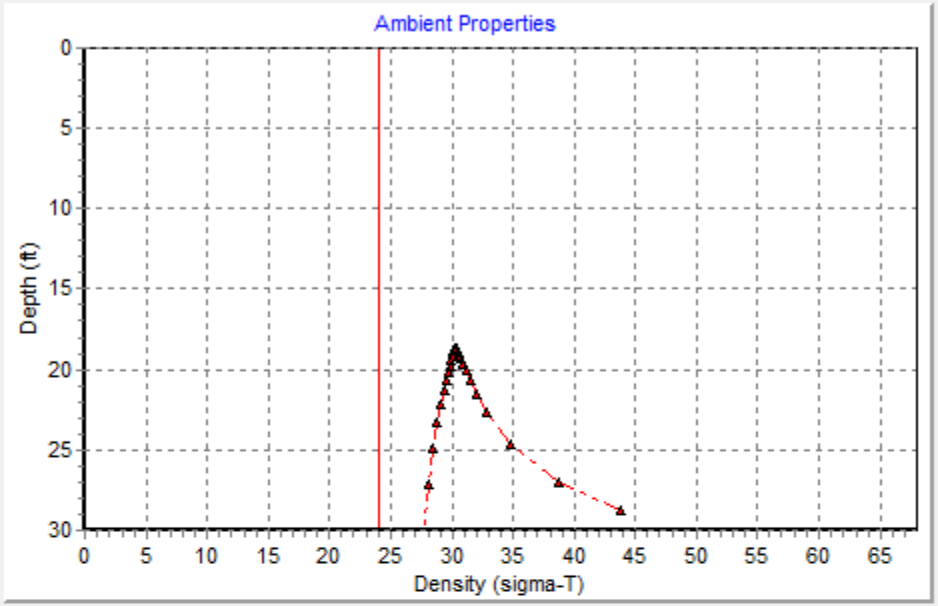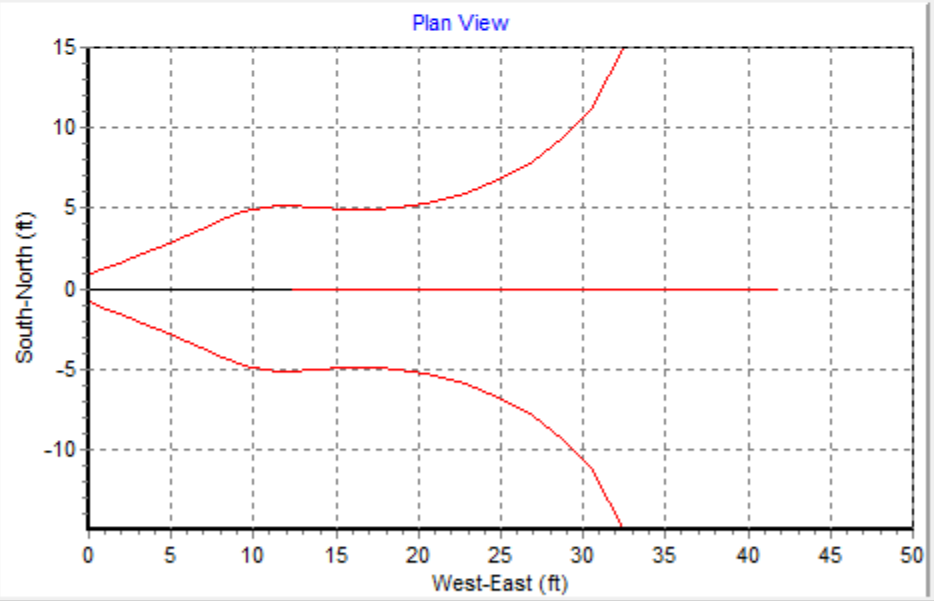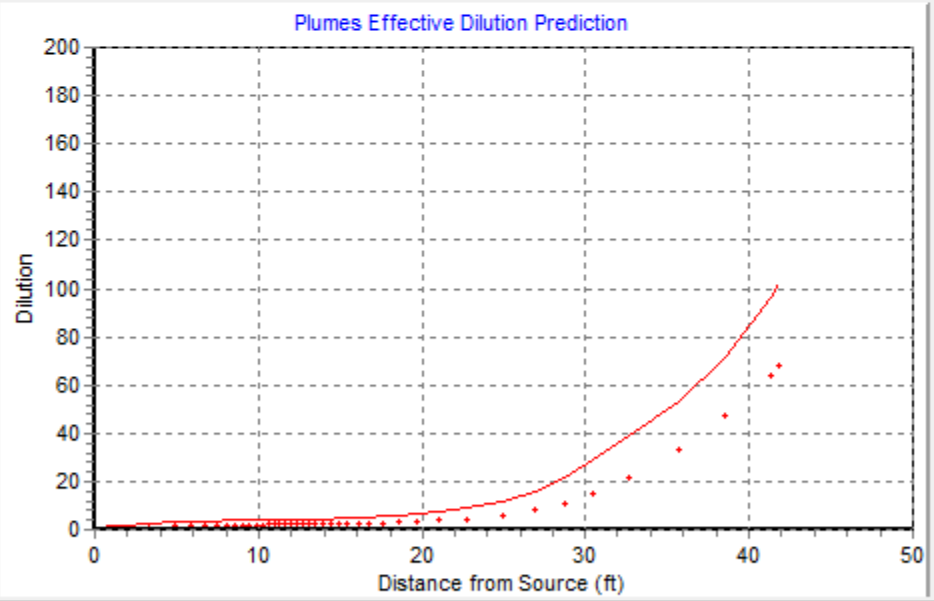
Plane